iScience

CellPress
OPEN ACCESS

Article

An electro-optical platform for the ultrasensitive detection of small extracellular vesicle sub-types and their protein epitope counts

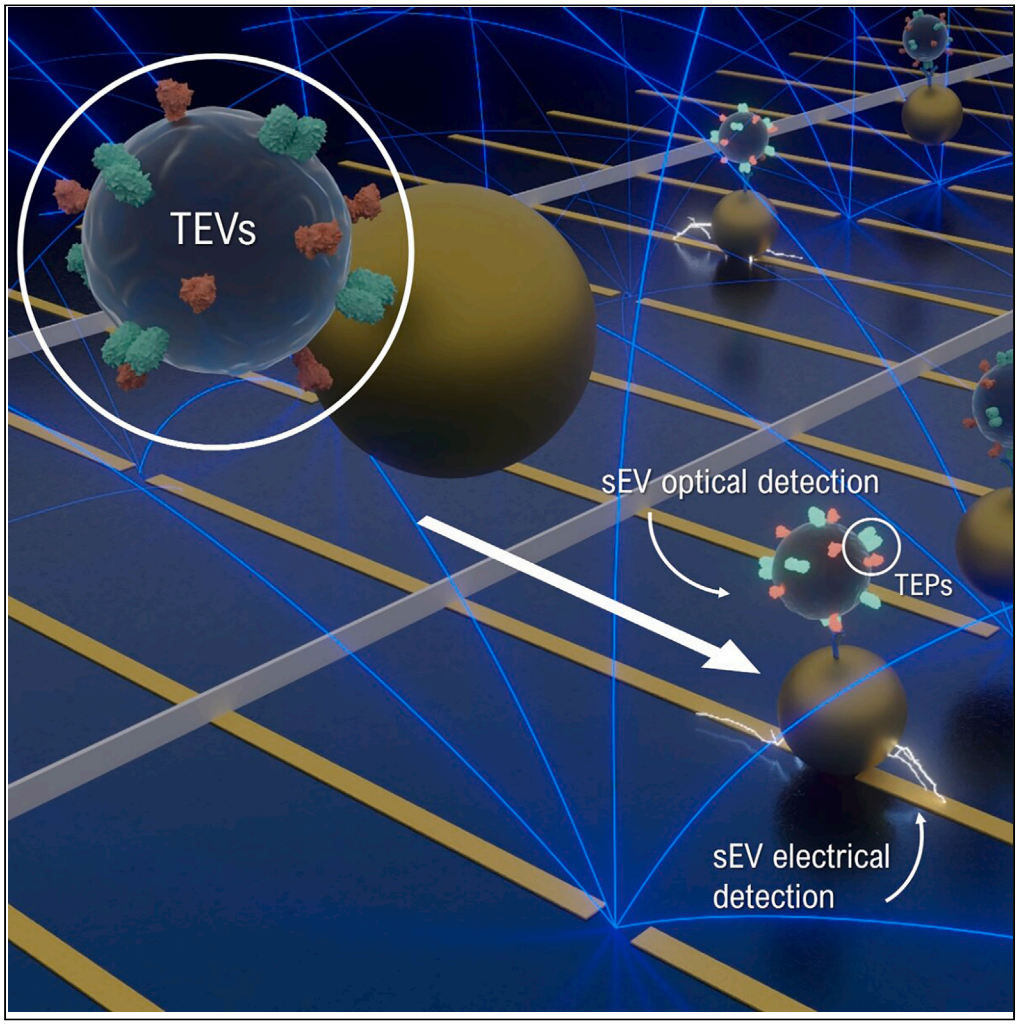

Tomás Dias, Ricardo Figueiras, Susana Vagueiro, ..., Jagriti Sethi, Elnaz Persia, Pierre Arsène

tomas.dias@mursla.com

Highlights

Novel NEXOS platform quantifies target small EV (sEV) sub-types and protein biomarkers

Combining electrical and optical NEXOS advances the phenotyping of sEVs in biofluids

E-NEXOS and O-NEXOS show superior detection limits compared to popular detection tools

NEXOS sets the basis for counting proteins on sEV sub-types at low concentrations

Its features may reveal new biological insights and drive the clinical adoption of sEVs

Dias et al., iScience *27*, 109866
June 21, 2024
https://doi.org/10.1016/j.isci.2024.109866

iScience

CellPress
OPEN ACCESS

Article

An electro-optical platform for the ultrasensitive detection of small extracellular vesicle sub-types and their protein epitope counts

Tomás Dias,[1,3,*] Ricardo Figueiras,[1,2] Susana Vagueiro,[1,2] Renato Domingues,[1,2] Yu-Hsien Hung,[1,2] Jagriti Sethi,[1,2] Elnaz Persia,[1] and Pierre Arsène[1]

SUMMARY

Methods for detecting proteins in small extracellular vesicles (sEVs) lack sensitivity and quantitative accuracy, missing clues about health and disease. Our study introduces the Nano-Extracellular Omics Sensing (NEXOS) platform, merging electrical (E-NEXOS) and optical detection (O-NEXOS). E-NEXOS determines the concentration of target sEV sub-types, and O-NEXOS quantifies the concentration of target protein epitopes (TEPs) on those TEVs. In this work, both technologies were compared to several sEV detection tools, showing superior detection limits for $CD9^+CD81^+$ and $CD9^+HER2^+$ sEVs. Furthermore, the additional information on TEVs and TEPs from bulk sEV samples, provided new phenotyping capabilities. We determined the average number of CD81 and HER2 proteins on $CD9^+$ sEVs, a number which was later validated on spiked human plasma. These results highlight the compatibility of NEXOS with complex biofluids and, as importantly, hint at its many potential applications, ranging from basic research to the anticipated clinical translation of sEVs.

INTRODUCTION

Small extracellular vesicles (sEVs) are membrane-enclosed vesicles secreted by cells transporting nucleic acids, proteins, lipids, and metabolites, and have emerged as significant actors in intercellular communication.[1,2] sEVs contribute to a wide range of biological processes in health[3] and disease[3] and are being widely explored in various applications from diagnostics to therapeutics.[4,5]

Currently, samples containing sEVs are routinely characterized for particle size and concentration using well-established techniques such as nanoparticle tracking analysis (NTA) or tunable resistive pulse sensing (TRPS). However, these methods are ineffective at distinguishing sEVs from other circulating particles such as lipoproteins and protein aggregates.[6]

Usually, techniques such as enzyme-linked immunosorbent assay (ELISA), western blot (WB) or bead-based flow cytometry (FCM) are routinely used for detecting the presence of sEVs and, more concretely, the presence of protein biomarkers on sEVs and of specific sEV sub-types, i.e., containing a subset of protein markers and normally co-existing with other sub-types in sEV samples (or mixtures).

Despite their usefulness in routine research, these methods lack the resolution and sensitivity likely needed to detect sEV surface proteins, beyond the commonly targeted markers (e.g., CD9, CD81, CD63, and CD41), making them unsuitable for revealing unknown biological processes or for their application in clinical sciences.[4,7]

More recently, single sEV analysis methods such as imaging flow cytometry (IFC), nanoparticle flow cytometry (NFCM) and single-particle interferometric reflectance imaging sensor (SP-IRIS) have emerged. These methods have shown promising features but still suffer from insufficient sensitivity, specificity, and precision, as widely discussed in literature.[4,7,8]

Briefly, they report signal outputs in relative arbitrary units which cannot effectively be translated to concentrations of sEV sub-types or protein biomarkers. Additionally, they lack reproducibility at sEV concentrations of 1E7 part/mL and lower making them unattractive for clinical diagnostics.[7–9] As an example, it is now recognized that the concentration of sEVs in blood is at least 1000 times lower than that of other blood particles, and sEVs originating from vital organs or tissues make up about 0.2% of their total count.[10,11]

Typically, this results in sEV sub-types with fewer than 1E7 particles/mL which may carry undiscovered biological significance.

As a result, there is a scarcity of methods offering quantitative analyses at low sEV concentrations. Such methods would advance our understanding of the biological role of sEVs and support their translation into clinical applications.[12] In this study, we introduce Nano-Extracellular Omics Sensing (NEXOS), a platform for ultrasensitive and phenotypic characterization of target sEV sub-types (TEVs) and their protein markers.

[1]Mursla Bio, Cambridge, UK
[2]These authors contributed equally
[3]Lead contact
*Correspondence: tomas.dias@mursla.com
https://doi.org/10.1016/j.isci.2024.109866

NEXOS comprises a nanoelectronics technology, Electro-NEXOS (E-NEXOS), and a high-throughput optical technology, Optical-NEXOS (O-NEXOS). E-NEXOS utilizes dielectrophoretic (DEP) forces for the attraction and detection of gold nanoparticles (GNPs).[13] The detected GNPs are pre-bound to TEVs, which enables determining the concentration of TEVs via the pre-establishment of the stoichiometric ratio between GNPs and TEVs.

O-NEXOS is designed for determining the concentration of Target protein Epitopes (TEPs) in said TEVs, via optical labeling. The integration of E-NEXOS and O-NEXOS into a unified platform provides a more comprehensive assessment of EV sub-types. O-NEXOS technology has been previously employed for the qualitative detection of $CD41^+$ sEVs in serum and plasma, however, here we sought to improve it for the determination of TEP concentrations in sEV mixtures.[14] The density of TEPs has been reported before in an attempt to standardize the reporting of sEV results when using different FCM platforms.[15,16] Nonetheless, we show here for the first time, a method for determining the concentration of TEVs, TEPs and the average number of protein epitopes per sEV sub-type (TEPs/TEVs) in sEV mixtures.

Our aim with NEXOS is not only to demonstrate high sensitivity in detecting sEVs but, as importantly, to address unmet quantification features that could help revealing unknown biological significance of sEVs. Some of the unmet quantification features are the concentration determination of specific sEV sub-sub-types in simple and complex fluids, the concentration of specific sEV markers and the abundancy of those markers per sEVs of interest.

In this study, we presented the core operating principles of E-NEXOS and O-NEXOS, followed by the characterization of the sEVs utilized herein. These sEVs were derived from two specific breast cancer cell lines, MCF-7 and BT-474. Our goal was to characterize two distinct sEV sub-types: a traditional sub-type associated to both cell lines, namely $CD9^+CD81^+$ sEVs and a cancer-associated sub-type, $CD9^+HER2^+$ sEVs found predominantly in samples derived from HER2-overexpressing tissues and cell lines, like BT-474.

Given the innovative feature of E-NEXOS, we delved into its sensing mechanism, optimization and stoichiometric validation needed for determining the concentration of TEVs. The method was developed using $CD9^+CD81^+$ MCF-7 sEVs and applied to the characterization of $CD9^+CD81^+$ and $CD9^+HER2^+$ sub-types derived from BT-474 sEVs.

We reported for both technologies, a signal variation proportional to the serial dilution of sEVs in PBS and spiked in human plasma. In addition, we determined the corresponding concentration of the sEV sub-types in the original sEVs mixture and of their target biomarkers, namely CD81 and HER2.

Also, we determined the average quantity of CD81 and HER2 protein markers present in those TEVs (TEPs/TEVs), with concordant results obtained between simple mixtures and spiked plasma.

Finally, we demonstrated the superior sensitivity of E-NEXOS and O-NEXOS compared to that of widely-used sEV detection tools.

Ultimately, this manuscript introduces a new methodology for characterizing sEVs, with an approach particularly useful for low concentration ranges, where current methods fall short in characterizing sEVs beyond the detection of their relative signals.

With the maturation of the NEXOS technologies, we briefly entice interest in their upcoming stages which are expected to result in unparalleled sensitivity and clinical applicability.

RESULTS

Working principle of NEXOS

The general workflow of the NEXOS platform is illustrated and summarized in Figure 1.

TEVs are labeled with "detection" biotinylated antibodies, recognizing a target surface protein on sEVs (Figure 1A). Next, sEVs are captured on antibody pre-coated magnetic beads (MBs) recognizing a specific capture marker (Figure 1B).

Unbound detection antibodies and non-target sEVs are washed away in a magnetic field (Figure 1B).

For O-NEXOS, a polymerized form of horseradish peroxidase (HRP) covalently bound to streptavidin (S-polyHRP), enabling signal amplification, is incubated with the captured sEVs. Signal is acquired after washing and addition of a fluorescent substrate, after which the concentration of TEPs is extrapolated from fluorescent readings (Figure 1C).

For E-NEXOS, 200 nm streptavidin-coated GNPs (S-GNPs) are incubated with the EVs captured on the MB, resulting in the formation of MBs-sEVs-S-GNPs complexes, via streptavidin-biotin coupling (Figures 1D–11). Unbound S-GNPs are washed away in a magnetic field and the bound S-GNPs are eluted from the MBs using a 0.2 M Glycine (pH 2.6) solution, adapted from previously validated methods (Figures 1D and 2).[17,18] The recovered S-GNPs are washed using centrifugation and buffer is exchanged to a low conductivity buffer. Finally, indirect detection of TEVs is achieved via quick attraction by DEP and detection of eluted S-GNPs on the E-NEXOS nanochip (Figures 1D and 3).

sEVs show size, morphology, typical markers and the exclusive detection of HER2 in BT-474

For the proof-of-concept and validation of NEXOS, sEVs were prepared from the conditioned media of MCF-7 (ATCC HTB-22), a low-grade luminal A non-metastatic breast cancer cell line, and BT-474 (ATCC HTB-20), an HER-2 overexpressing breast cancer cell line (see details in Materials and methods).[19,20] The cell-derived sEVs were characterized according to current standards in the field for validation.[21] Particle numbers were quantified by NTA (Figure 2A). The presence of the sEV specific antigens, CD9, CD81, CD63 and TSG101 were detected by WB (Figure 2B) and the presence of CD9, CD81 and CD63 was further confirmed by FCM (Figures 2D and 2E). The spherical shape and lipid bilayer membrane was established by Transmission Electron Microscopy (TEM) (Figure 2C). HER2 antigen was not detected in MCF-7 sEVs, while it was confirmed to be present in sEVs isolated from BT-474, again by WB and FCM (Figures 2B and 2E).

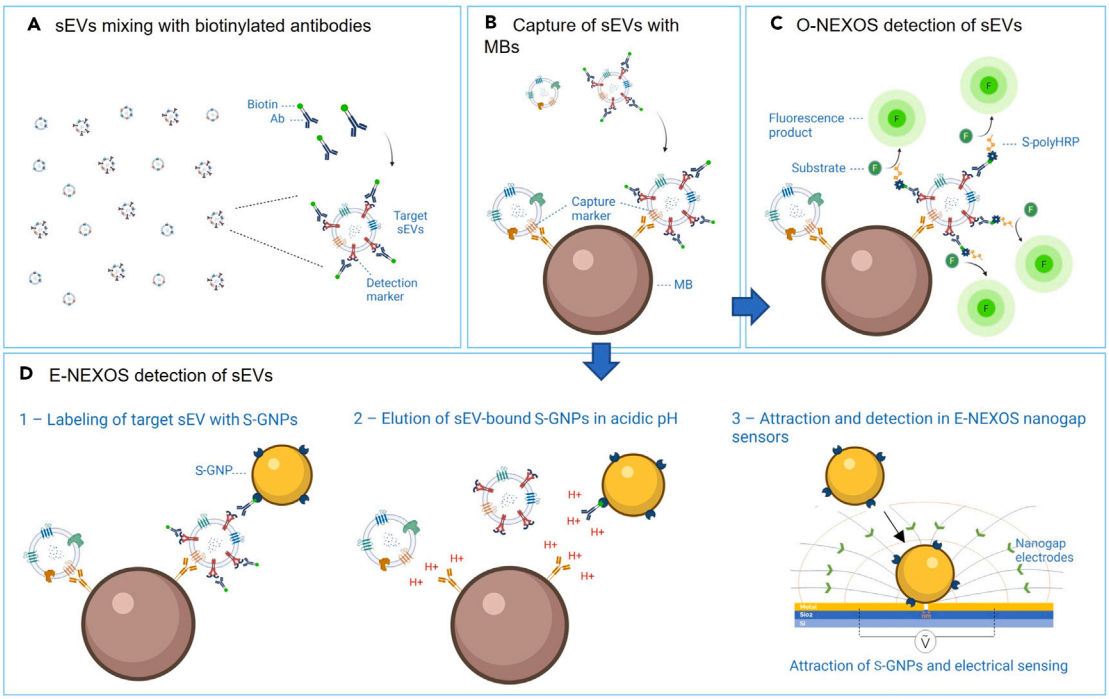

Figure 1. NEXOS workflow for the detection of sEVs

(A) Biotinylated (detection) antibodies recognize and bind to target surface proteins (detection markers) on sEVs.

(B) Magnetic beads (MBs) pre-coated with (capture) antibodies, capture (detection) antibody-labeled target sEVs and non-labeled sEVs.

(C) O-NEXOS detection of target sEV epitopes is performed by the stepwise addition of S-polyHRP and fluorescence substrate followed by measurement of the resultant fluorescence product.

(D) Alternatively, E-NEXOS is performed by 1- adding streptavidin-GNPs (S-GNPs) to the mixture of MB-captured sEVs. sEV-bound GNPs are recovered by washing the MBs-sEVs-S-GNPs complexes in a magnetic field. 2 – S-GNPs are eluted by dissolving the complexes in pH 2.6. 3 – Buffer containing S-GNPs is exchanged by centrifugation to a low conductivity buffer and, finally, the S-GNPs are attracted and detected on an E-NEXOS nanochip. See also Figure S1.

E-NEXOS demonstrates unbiased detection of S-GNPs across a four-Log concentration range

In Figure 1, the workflow of NEXOS technology is summarized (Figures 1D and 3).

The detailed description of the chip fabrication process is available in the 'materials and methods' section. Briefly, chips were fabricated using an n-doped silicon wafer in a two-layer configuration. Each layer underwent meticulous lithography and metal deposition steps. The nanogaps were fabricated in the first layer and contact lines and pads were fabricated in the second layer. The nanochips were fabricated with a dimension of 12 × 12 mm^2 and contain 36 nanosensors distributed in 4 sensing areas with 9 sensors each (Figure 3A). To expand the attraction surface area, each sensor consisted of 3 parallel electrode pairs (Figure 3B) made with a layer of Ti5/Au30 (thicknesses in nm), a width of 300 nm and a nanogap separation of 50 nm (Figure 3C). The S-GNPs are attracted to the nanogap via "sink effect" resulting from the application of an AC voltage across the electrodes pair, which generates a non-uniform electric field perpendicular to the nanogaps. This field polarizes S-GNPs in the vicinity with a positive DEP force. Considering the nanosensors' geometric parameters, we simulated the cross-sectional gradient of the electric field intensity, $\nabla|E^2|$, generated by 2 V AC at 100 kHz in the vicinity of a nanogap using the COMSOL Multiphysics software.

The simulation revealed that the highest $\nabla|E^2|$ is at the edge of the electrodes and it decreases proportionally with the distance from the nanogap (Figure 3D).

Subsequently, we conducted experimental tests under the simulated conditions (2 V AC, 100 kHz). We fine-tuned the DEP trapping process for the efficient capture of S-GNPs pre-bound to sEVs. The capture was validated using Scanning Electron Microscopy (SEM), offering a direct visualization of S-GNPs on the nanogaps (Figure 3E). Detailed experimental information are provided in the supplementary information, materials and methods and in referenced patents.[22,23]

Briefly, to sense the attracted S-GNPs, chips were cleared from any liquid, dried and then activated with an electrical potential of 5 V DC.

After activation, we observed a shift in current from pA (open-circuit) up to mA (closed-circuit) on all nanogap sensors that were bridged by an S-GNP. Conversely, the sensors with no S-GNPs attached continued displaying currents in pA range (See also illustration in Figure S1).

This procedure promoted a significant current shift of nine-orders of magnitude (from pA to mA) which resulted in the unbiased detection of S-GNPs (Figure 3F).

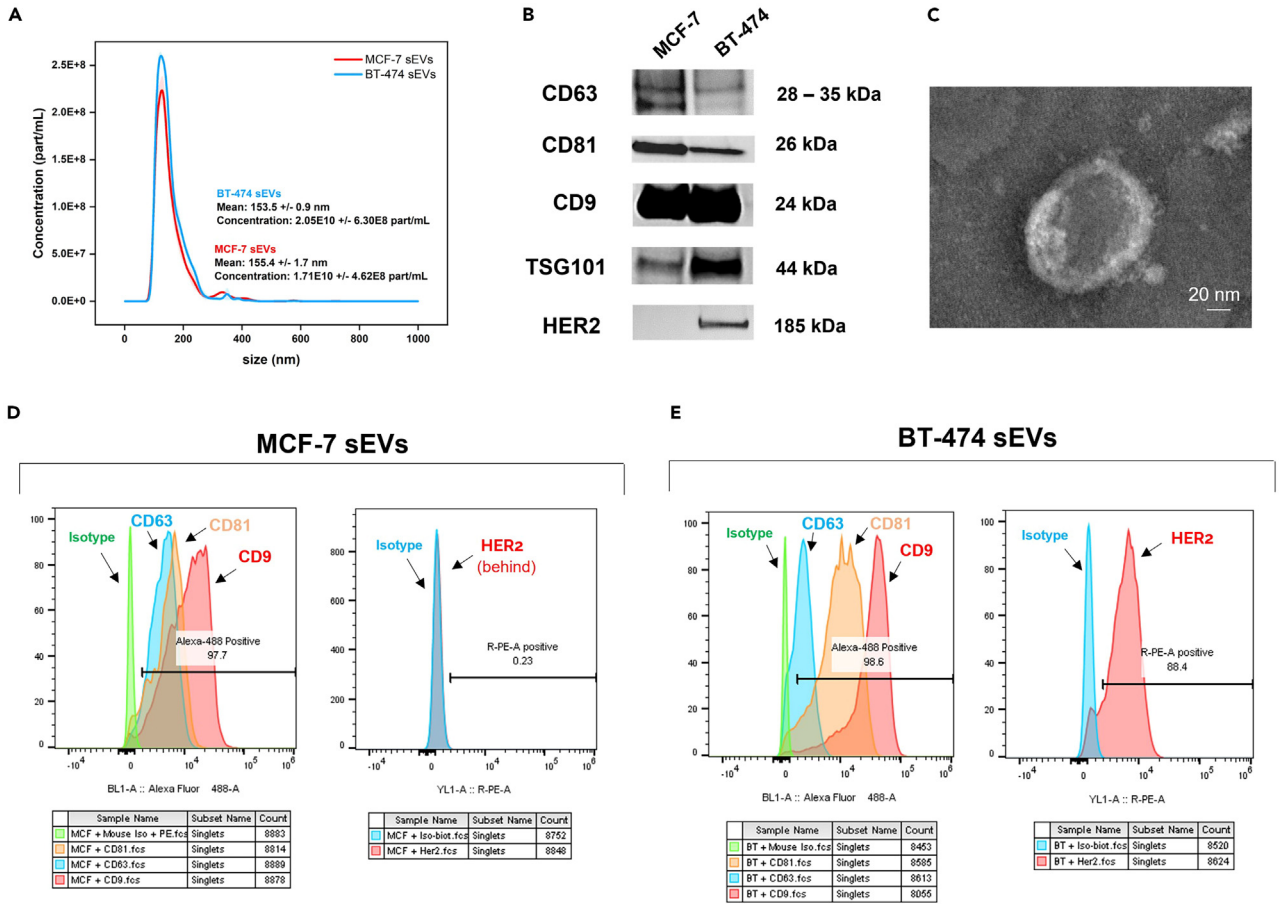

Figure 2. Characterization of MCF-7 and BT-474 sEVs

(A) Average diameter and particle concentration of pre-prepared MCF-7 and BT-474 sEVs, as determined by NTA (n = 3).

(B) Western blot analysis of CD63, CD81, CD9, TSG101 and HER2 in lysates of MCF-7 and BT-474 sEV preparations.

(C) Size and morphological characterization of BT-474 sEVs by transmission electron microscopy (TEM).

(D and E) Determination of CD63, CD81, CD9, and HER2 proteins in MCF-7 and BT-474 sEVs by bead-based flow cytometry (FCM).

The percentage of S-GNPs hits (%) in each nanochip was determined using Equation 1. The equation calculates the percentage of nanosensors bridged by S-GNPs in function of the number of viable nanosensors on the E-NEXOS nanochips:

$$\text{Hits } \% = \frac{\text{N° connected sensors}}{\text{N° total sensors}} * 100 \qquad \text{(Equation 1)}$$

We optimized different experimental parameters, and investigated their impact on the hits %. This involved testing S-GNPs with different diameters: 100 nm and 200 nm; different attraction voltages: 0.8 V(100 kHz), 2 V AC (100 kHz) and 4 V (100 kHz); and solutions for eluting the S-GNPs: Ultra-pure water and 1% PBS.

The highest sensitivity was achieved with S-GNPs of 200 nm and by using an attraction voltage of 2 V AC (100 kHz) (Figures S2A and S2B). The overall sensitivity could technically be improved with 4 V (100 kHz) but we observed partial destruction of nanosensors above 2 V AC (data not shown).

When selecting the optimal solution for eluting S-GNPs, we realized we could detect 4 concentration logs by using both ultra-pure water and 1% PBS for different S-GNP concentrations (Figure S2C). With that, we established two detection modes: a low range (LR) mode (using ultra-pure water) and a high range (HR) mode (using 1% PBS) (Figures S2D and S2E), leading to a dynamic concentration range between 7.5E4 and 1E8 part/mL. A calibration curve correlating the hits % with the concentration of S-GNPs was established, considering the two modes of operation (Figure 3G).

The integration of an immunomagnetic assay in NEXOS workflow enabled the linear detection of sEV sub-types

Since E-NEXOS quantifies S-GNPs and O-NEXOS measures the concentration of S-polyHRP, we aimed to develop an immunomagnetic assay to efficiently separate sEV-bound from unbound S-GNPs and S-polyHRP for E-NEXOS and O-NEXOS detection, respectively.

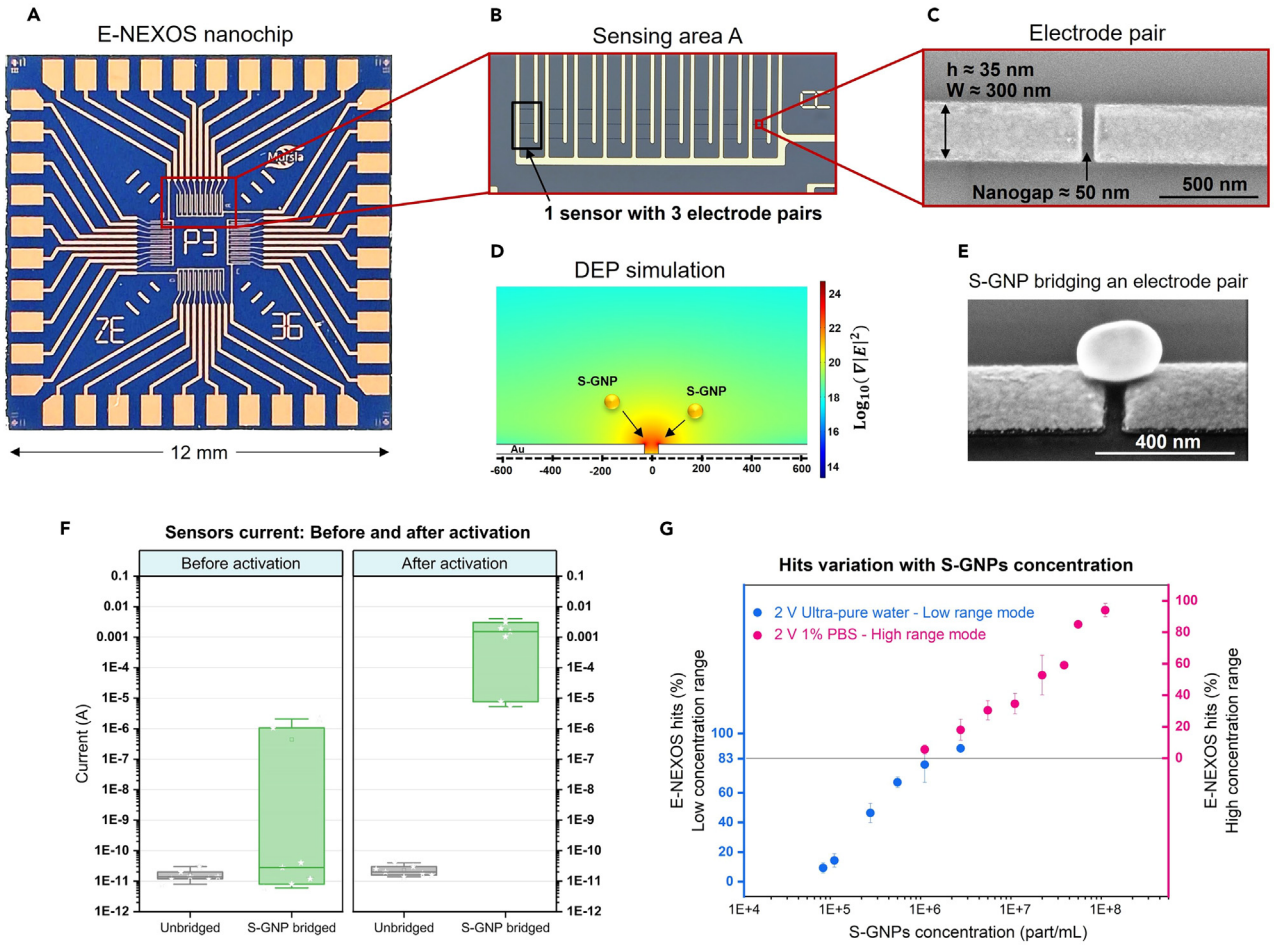

Figure 3. E-NEXOS design and sensing principle

(A) Optical images of an E-NEXOS nanochip with 36 sensors divided into 4 sensing areas.

(B) Optical images of a sensing area in E-NEXOS nanochip. Each area contains 9 sensors with 3 nanogaps each.

(C) Characterization of a nanogap by scanning electron microscopy (SEM). The measured dimensions of the nanogap and gold electrodes are described.

(D) Simulation of the gradient of the electric field intensity $\nabla|E^2|$ in a nanogap, using the nanogap dimensions and electrical parameters used experimentally. Nanoparticles placed under this field experience a positive dielectrophoresis (DEP) force, being attracted to the nanogap.

(E) SEM characterization of an electrode pair separated by a nanogap after attracting S-GNPs and showing an attracted S-GNP bridging the nanogap.

(F) Current measured on unbridged nanogaps and on nanogaps after trapping S-GNPs, before and after activation with 5 V DC (n = 7). Data are mean ± S.D.

(G) Determination of hits % in E-NEXOS in function of S-GNPs concentration in the low range (LR) and high range (HR) sensitivity modes (n = 4). Data are mean ± S.D. See also Figure S2.

The immunomagnetic assay consisted of 2.8 μm MB pre-coated with anti-CD9 or anti-CD81 antibodies. We determined the antibody coating efficiency with a Bicinchoninic acid (BCA) protein assay, and obtained good correlation with the values estimated by the supplier (Figure S3A). An average coverage of approximately 3.1E5 anti-CD81 and 4.5E5 anti-CD9 antibodies per MB was achieved (Table S1), suggesting that the MBs possessed high affinity to $CD9^+$ and $CD81^+$ sEVs.

The efficiency for capturing sEVs was validated with pre-enriched $CD9^+$ MCF-7 sEVs (refer to Materials and Methods and SI for details). Using the pre-enriched sub-population, we determined a capture efficiency rate of 97%, confirming the high affinity of the immunomagnetic assay for targeted sEVs (Figure S3B).

To test the integration of the immunomagnetic assay in E-NEXOS, sEVs derived from MCF-7 were serially diluted to concentrations ranging from 5E8 down to 5E6 part/mL. Biotinylated anti-CD81 antibody was coupled to the sEVs before being captured with MBs anti-CD9 or isotype IgG. The captured sEVs were labeled with 200 nm S-GNPs or S-polyHRP. A volume of 45 μL was spotted on the surface of E-NEXOS nanochip and each sensor was exposed to a DEP potential of 2 V AC (100 k) for a duration of 1 min, after which the liquid was removed. The nanosensors with attracted S-GNPs were activated by applying 5 V DC for 20 s and their sensing was performed with a sweeping voltage from 0 to 5 V DC.

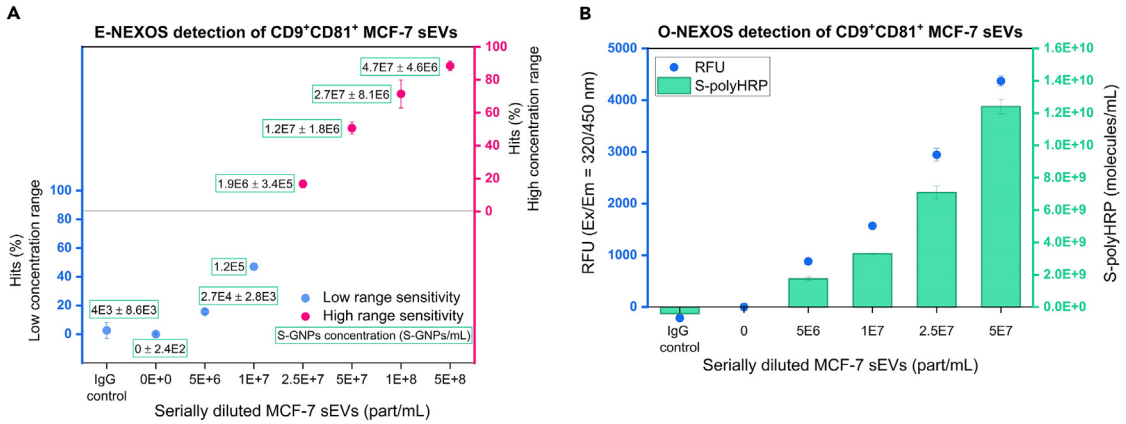

Figure 4. The integration of sEVs capture with MBs enables the detection of sEVs with E-NEXOS and O-NEXOS

(A) E-NEXOS detection of pre-prepared bulk MCF-7 sEVs by their capture with MBs pre-coated with anti-CD9 antibody and detection with S-GNPs targeting CD81 antigens on the sEVs at various concentrations. The measurements were obtained in the HR and LR sensitivity modes of E-NEXOS (n = 4) Data are mean ± S.D. The measurements included controls with anti-CD9 MBs and without sEVs (blank) and MBs pre-coated with igG antibodies and sEVs at a concentration of 5E8 part/mL (IgG control).

(B) O-NEXOS detection of pre-prepared bulk MCF-7 sEVs by their capture with MBs pre-coated with antibody anti-CD9 and reporting via S-polyHRP detection upon its binding to biotinylated antibodies anti-CD81. The graph includes the fluorescence signal detected (left y axis) and the determined number of S-polyHRP per reaction (right y axis) (n = 4) Data are mean ± S.D. The measurements included controls with anti-CD9 MBs and without sEVs (blank) and MBs pre-coated with igG antibodies and sEVs at a concentration of 5E8 part/mL (IgG control). See also Figure S3 and Table S1.

We observed that the number of hits % proportionally increased with the concentration of sEVs on both LR and HR modes (Figure 4A). Using the calibration curve derived from Figure 3G, the concentration of S-GNPs bound to $CD9^+CD81^+$ sEVs was determined (graph inset values, Figure 4A).

Similarly to E-NEXOS, we observed a linear response in fluorescence signal with that of sEV concentrations in O-NEXOS (left y axis in Figure 4B).

By plotting a calibration curve (Figure S4), we also correlated the fluorescence signal with the concentration of S-PolyHRP (right y axis in Figure 4B).

The association between hits % with S-GNP concentrations and of fluorescence signal with S-polyHRP concentrations was essential to later determine TEV and TEP concentrations.

Determining the stoichiometry of S-GNPs to sEVs calibrated and validated E-NEXOS for TEV analysis

As the E-NEXOS readout is represented as a percentage of nanogaps bridged by S-GNPs (hits %), and this percentage is directly linked to the concentration of S-GNPs, we initially calculated the average count (or ratio) of S-GNPs binding to one sEV in the immunoassay. This calculation was motivated by the potential establishment of a direct relationship between the concentration of S-GNPs and TEVs.

For that, we hypothesized that the number of S-GNPs capable of binding to a single sEV captured on the MBs is limited by the larger size of S-GNPs (~200 nm) compared to sEVs (100 nm in average), regardless of the number of target protein epitopes existing in a target sEV.

We conducted a theoretical analysis to determine the maximum number of S-GNPs that can attach to sEVs when the later are pre-captured on the surface of MBs, in agreement with the immunoassay. Our calculations revealed that the stoichiometry between S-GNPs per sEVs, could be no more than two S-GNPs bound per one sEV, assuming an sEV average diameter of 100 nm (Table S2).

Next, we aimed to determine experimentally the number of S-GNPs bound per sEV on a sample pre-enriched in a sub-population of $CD81^+CD9^+$ MCF-7 sEVs.

The enrichment was performed by the capture and elution of MCF-7 sEVs, first with MBs pre-coated with antibody anti-CD9 and after, with MBs pre-coated with antibody anti-CD81.

The elution of target sEVs after each capture step was performed in 0.2 M Glycine pH 2.6 as previously reported (refer to Materials and Methods).

The enriched $CD9^+CD81^+$ sEVs preparation was serially diluted from a starting concentration of 1E8 part/mL down to 1E6 part/mL for E-NEXOS detection. The S-GNPs bound to sEVs were recovered and their concentration was determined via the hits % resulting from the E-NEXOS measurements. The hits % were converted to concentration units via the calibration demonstrated in Figure 3G.

As observed in Figure 5A, the concentration of S-GNPs increased proportionally with the concentration of sEVs, both in the LR and HR detection modes (inset values show the corresponding hits %). Considering the pre-enrichment of $CD9^+CD81^+$ sEVs, we formulated a logistic equation to obtain the relationship between the concentration of S-GNPs and TEVs across the different serial dilutions (Figure 5B).

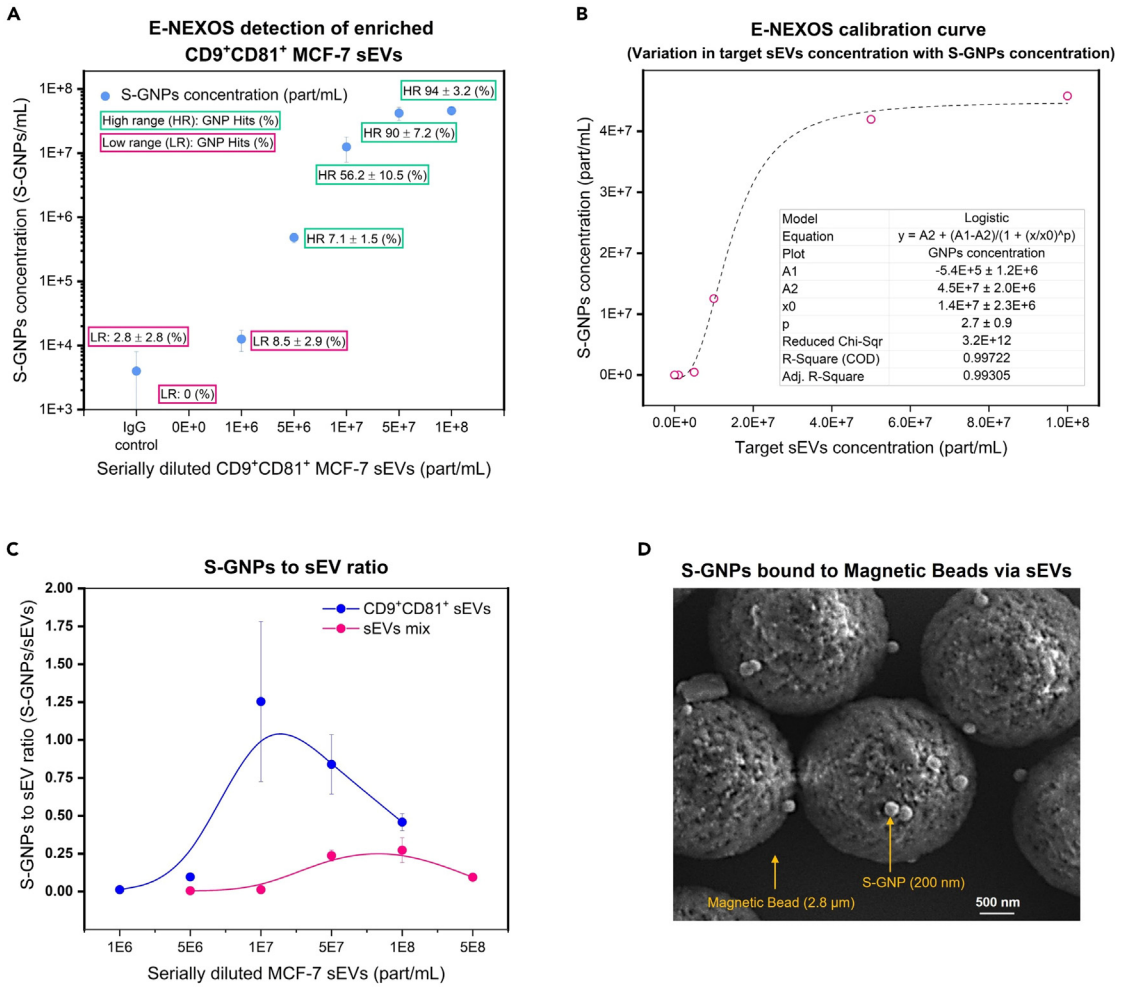

Figure 5. Determination of TEVs

(A) E-NEXOS detection of enriched CD9$^+$CD81$^+$ MCF-7 sEVs by the capture of CD9$^+$CD81$^+$ MCF-7 sEVs with MBs pre-coated with anti-CD9 antibody and detection with S-GNPs targeting CD81 antigens on the sEVs at serially diluted sEV concentrations. The measurements were performed using LR and HR modes of E-NEXOS (n = 4). Data are mean ± S.D. The measurements included controls with anti-CD9 MBs and without sEVs (blank) and MBs pre-coated with igG antibodies and sEVs at a concentration of 5E8 part/mL (IgG control).

(B) E-NEXOS is calibrated by pre-enriching CD9$^+$CD81$^+$ MCF-7 sEVs and detected at serially diluted sEV concentrations. A calibration curve enabling the derivation of the concentration of TEVs is determined as a function of the concentration of S-GNPs (n = 4).

(C) Determination of the ratio and standard deviation of S-GNPs bound per sEV in a mixture of sEVs (graph – pink line) and in a population enriched in CD9$^+$CD81$^+$ sEVs (graph – blue line) Data are mean ± S.D.

(D) Characterization by SEM of magnetic beads and S-GNPs after E-NEXOS bioassay with CD9$^+$CD81$^+$ sEVs (5E6 EVs/mL). The characterization confirms the ratio of S-GNPs to sEVs is either one or two S-GNPs per sEV at the concentration tested. See also Table S2.

The relationship resulted in a varying ratio between S-GNPs and sEVs at different concentrations (Figure 5C). Interestingly, at a concentration of 1E7 sEVs/mL, we obtained a ratio of 1.3 ± 0.5 S-GNPs/sEVs, which corroborated with our analysis that no more than two S-GNPs could be bound to one sEV (Table S2).

As expected, lower ratios were observed without prior TEV enrichment, underscoring the importance of calibrating and validating the technology with pre-enriched samples for TEV characterization in sEV mixtures (Figure 5C).

The ratio between s-GNPs and sEVs was further confirmed by SEM, via the observation of S-GNPs clusters with no more than two S-GNPs after an E-NEXOS bioassay (Figure 5D).

Quantifying TEVs and TEPs in distinct sEV sub-types enables epitope counting in sEV mixtures

After obtaining a model to correlate the concentration between S-GNPs and TEVs (Figure 5B), we formulated an equation to estimate the concentration of TEPs. This calculation was based on the concentration of S-polyHRP and its correlation with fluorescence signal, as shown

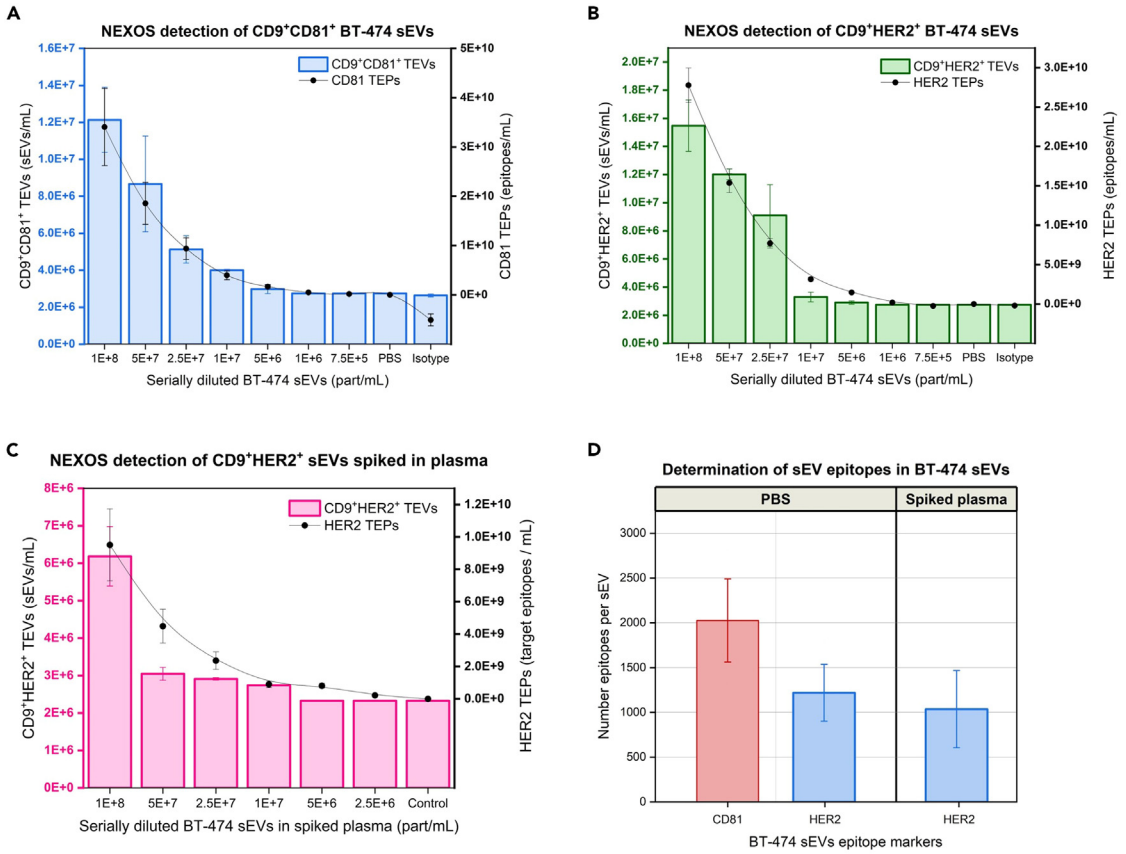

Figure 6. Analytical detection and characterization of target sEVs (TEVs), target epitopes (TEPs) and epitopes per sEV in BT-474 sEVs

(A) Analytical detection of $CD9^+CD81^+$ BT-474 sEVs and determination of $CD9^+HER2^+$ TEVs (E-NEXOS) and HER2 TEPs (O-NEXOS) at serially diluted BT-474 sEV concentrations (n = 4).

(B) Analytical detection of $CD9^+HER2^+$ BT-474 sEVs and determination of $CD9^+HER2^+$ TEVs (E-NEXOS) and HER2 TEPs (O-NEXOS) at serially diluted BT-474 sEV concentrations (n = 4).

(C) Analytical detection of $CD9^+HER2^+$ BT-474 sEVs spiked in processed plasma and determination of $CD9^+HER2^+$ TEVs (E-NEXOS) and $HER2^+$ TEPs (O-NEXOS) at serially diluted BT-474 sEV concentrations in the spiked plasma (n = 4).

(D) Determination of CD81 and HER2 epitopes per BT-474 sEV, (n = 4). The measurements included controls with anti-CD9 MBs and without sEVs (PBS) and MBs pre-coated with igG antibodies and sEVs at a concentration of 5E8 part/mL (IgG isotype control) Data are mean ± S.D. See also Figures S4–S6.

in Figure S4. The equation included a probabilistic factor to account for the possible binding events between S-polyHRP and TEPs, as described in Equation 2 (for additional details, refer to Materials and Methods).

$$TEPs_{\text{(in assay)}} = 4.5 \pm 2.3 * S - polyHRP_{\text{(in assay)}} \quad \text{(Equation 2)}$$

To translate the characterization of TEVs and TEPs to another source of sEVs and to an additional sub-population of sEVs, we serially diluted BT-474 sEVs from a starting concentration of 1E8 part/mL down to 1E6 part/mL, for their characterization in PBS and spiked plasma.

The sEVs were labeled with biotinylated antibodies anti-CD81 or anti-HER2 and captured with MBs pre-coated with antibody anti-CD9 for the characterization of $CD9^+CD81^+$ and $CD9^+HER2^+$ sub-types.

Consistent with our previous findings, the concentration of S-GNPs (or hit percentage) and the fluorescence signal for both $CD9^+CD81^+$ and $CD9^+HER2^+$ sub-types were directly proportional to the concentration of sEVs, with the latter also being tested in spiked plasma.

The limit-of-detection (LOD) achieved with O-NEXOS was 1E6 part/mL, and with E-NEXOS, it was 5E6 part/mL of the original sEV mixtures (Figure S5). Nevertheless, we determined the corresponding TEVs and TEPs concentrations for the two sub-types (Figures 6A–6C) which was consistent across concentrations for the linear regime of E-NEXOS. The sensitivity for $CD9^+HER2^+$ sEVs decreased by approximately 2–2.5 times when the sEV mixtures were spiked in plasma. This resulted in an LOD of 2.5E6 particles/mL for O-NEXOS and 1E7 particles/mL for E-NEXOS.

We calculated the ratio of S-GNPs to $CD9^+CD81^+$ and $CD9^+HER2^+$ BT-474 TEVs (Figure S6A) and their percentage in bulk BT-474 sEV mixtures (Figure S6B).

For that, we averaged the TEV concentrations that aligned with the linear regime of E-NEXOS, as per Figure 5B. Our findings indicated that, within our BT-474 sEV mixtures, 22.6 ± 5.4% of all the particles in the samples (sEVs and others) were positive for the co-expression of $CD9^+CD81^+$, while 31.1 ± 5.2% were positive for $CD9^+HER2^+$.

Considering the only difference between E-NEXOS and O-NEXOS bioassays is the choice of reporters utilized in the concluding step, but also considering that both the S-GNPs and S-polyHRP connect to the labeling antibodies via the same streptavidin-biotin interaction, we reasoned that the distinct observations provided by E-NEXOS and O-NEXOS could be combined to calculate the number of protein epitopes per detected TEV (TEPs/TEVs) without necessitating intricate adjustments. This level of straightforward integration is generally unfeasible with differing methodologies, as they typically employ different procedures and reagents which fundamentally dictate the kinetics of a bioassay. The protein counts of CD81 and HER2 per sEV were determined at sEV concentrations of 1E7, 1E8 part/mL and in between, as these concentrations were detected across the different experiments and, again, corresponded to the linear regime of E-NEXOS.

For BT-474 sEVs diluted in PBS, our analysis revealed an average count of 2027 ± 535 CD81 and 1220 ± 368 HER2 proteins in $CD9^+CD81^+$ and $CD9^+HER2^+$ sEVs, respectively. Likewise, in plasma spiked with BT-474 sEVs, we obtained an average of 1037 ± 522 HER2 proteins per spiked $CD9^+HER2^+$ sEV (Figure 6D). Interestingly, the quantity of HER2 protein epitopes remained consistent between the PBS and plasma measurements.

Validating the quantity of CD81 proteins in spiked plasma was not possible since the plasma of healthy donors naturally has $CD81^+$ sEVs while $HER2^+$ sEVs are restricted to patients with elevated HER2 levels.[24]

Collectively, these findings support the use of the methodology to determine the quantity of target proteins per target sEVs in simple and complex samples.

Compared to other technologies, O-NEXOS shows superior sensitivity followed by E-NEXOS

We compared the analytical range and LOD of O-NEXOS and E-NEXOS to that of established methods for sEVs characterization, namely Fluorescence-ELISA, IFC and SP-IRIS. During the serial dilution of BT-474 sEVs for E-NEXOS and O-NEXOS, we reserved ample sample volumes for concurrent tests with those techniques.

The sEV samples were sorted into multiple aliquots and promptly frozen at −80°C until needed.

Similarly to NEXOS, Fluorescence-ELISA and SP-IRIS employ two steps, one for the capture of sEVs and one for the detection of a marker of interest, while IFC exclusively stains sEVs for their direct detection without using a capturing step.

A commercially available ELISA kit, ExoELISA-ULTRA CD81 was chosen given its claimed high affinity and ultra-sensitivity.

SP-IRIS was done by capturing sEVs on ExoView chips via a CD9 antibody and detection via antibodies anti-CD81 or anti-HER2.

IFC was performed on an ImageStream X Mk II, and the sEVs were labeled with detection antibodies, anti-CD81 or anti-HER2.

We obtained a calibration curve for the ExoELISA-ULTRA CD81 kit using the standards and instructions provided by the supplier (Figure S7A). Using serially diluted BT-474 sEVs, ExoELISA-ULTRA CD81 kit detected sEVs down to a LOD of 1E10 part/mL (Figure S7B).

SP-IRIS detected sEVs down to a concentration of 1E7 part/mL, the smallest concentration tested (Figures S7C and S7D). The LOD of SP-IRIS was estimated to yield 9.4E6 part/mL for $CD9^+HER2^+$ sEVs and 4.7E6 part/mL for $CD9^+CD81^+$ sEVs (Figure S7E).

IFC detected CD81 and HER2 down to an LOD of 5E7 part/mL for both markers, albeit detecting more signal overall for HER2 (Figure S7F). Since IFC does not employ a capture step, the signal detected could originate in part from freely circulating proteins or protein aggregates. We did not pursue investigations in this regard, as it falls beyond the scope of the current study.

Finally, we compared the LOD of E-NEXOS and O-NEXOS with the tested techniques.

Overall, O-NEXOS demonstrated superior sensitivity all across followed by E-NEXOS (Figure 7). SP-IRIS matched the sensitivity of E-NEXOS for the detection of $CD9^+CD81^+$ sEVs but felled behind in the detection of $CD9^+HER2^+$ sEVs, alluring for E-NEXOS advantage in detecting sEVs with decreased number of TEPs, as per Figure 6D. This comparative analysis highlights NEXOS as a platform with superior sensitivity compared to the tested sEV methods.

DISCUSSION

This research was motivated by the need for more sensitive and more informative methods of characterizing sEVs.[25,26] EVs are gaining considerable significance for their promising impact in clinical sciences but, despite the plethora of methods available for detecting sEVs, there is none standing out with remarkable features.[25]

The established methods discussed in this study, are suitable for detecting traditional sEV biomarkers but provide limited information on the composition of sEVs in a sample. SP-IRIS is suitable for the co-localized detection of CD9, CD81 and CD63 on sEV samples but it does not inform on the actual concentration (nor percentage) of sEVs in a sample containing those markers. Indeed, SP-IRIS reports percentages but these only refer the relative percentage of CD9, CD81 and CD63 sEVs and sub-population combinations with these markers among each other and not to the total of particles in a sample. Also, although additional research is needed to further elucidate the role of these markers, it is unlikely they contain much value as biomarkers of health and disease.[27]

With NEXOS, we aimed to develop a platform that is suitable not only for the detection of non-traditional or undiscovered sEV markers in simple and complex fluids, but also for the characterization of sEV sub-types containing those markers.

The NEXOS platform results from the combination of two technologies, E-NEXOS and O-NEXOS, each aimed for distinct purposes. Nevertheless, they share an identical procedure with the only exception being the linking of sEVs to S-GNPs or S-polyHRP.

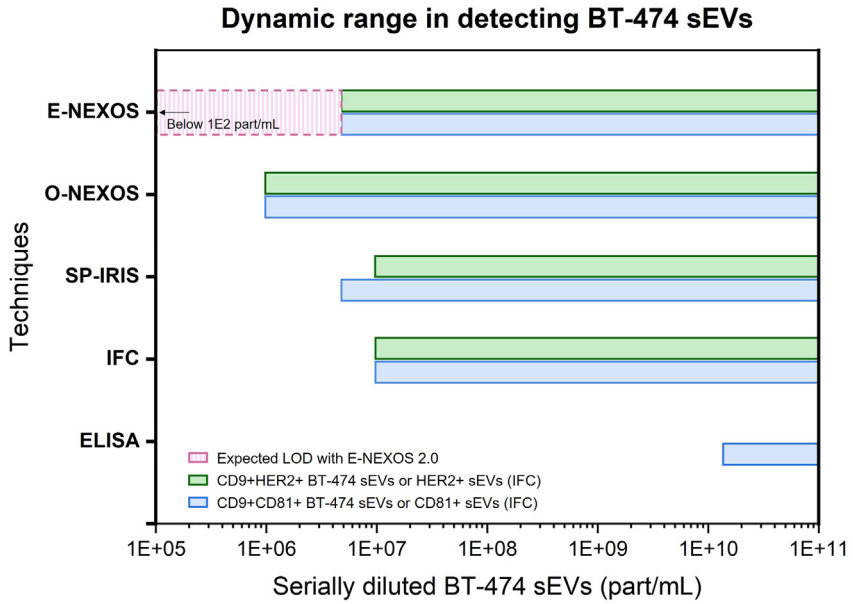

Figure 7. Comparison of different technologies for detecting serially diluted concentrations of BT-474 sEVs

Blue bars represent the lowest concentration of $CD9^+CD81^+$ or $CD81^+$ (IFC) sEVs achieved with each technique. Green bars represent the lowest concentration of $CD9^+HER2^+$ or HER2 (IFC) sEVs attained. The pink bar represents the promise of E-NEXOS next generation in achieving unmatched sensitivity by increasing the number of nanosensors per chip up to 1 million sensors. See also Figure S7.

NEXOS is completed with an immunomagnetic assay, which here has demonstrated a capture rate efficiency of 97% for $CD9^+$ MCF-7 sEVs, after a pre-enrichment step (Figure S3B).

The NEXOS methodology was first developed by targeting a $CD9^+CD81^+$ MCF-7 sub-population (Figure 4). Our data demonstrated the signal linearity of the methods in relationship to the concentration of sEVs.

To determine the concentration of TEVs, we assessed the number of S-GNPs that could bind to target sEVs in the immunomagnetic assay. Theoretical and experimental evidence agreed, as per the data in Table S2 and Figure 5. The stoichiometry was determined to be no more than two S-GNPs per sEV. Given the unchanging and straightforward relationship between sEVs and S-GNPs in the bioassay, we postulated that the relationship between any different sEV sub-population and S-GNPs of larger sizes should follow the correlation determined in Figure 5B.

We tested the method on $CD9^+CD81^+$ and $CD9^+HER2^+$ BT-474 TEVs and determined the quantity of these sub-types among the heterogeneous original BT-474 sEV mixtures (Figure S6B). With the presented results, we believe we pave the way for novel methodologies to characterize the concentration of particular sEV sub-types of interest (Figure 6).

Moreover, by combining E-NEXOS and O-NEXOS, we determined the quantity of protein epitopes per target sEV (TEPs/TEVs), specifically of CD81 and HER2. We showed the consistency of the method across simple and complex samples, evidenced by the comparable count of HER2 protein epitopes per sEV acquired (Figure 6D).

The comparison in sensitivity between E-NEXOS and O-NEXOS and that of widely-used sEV detection methods, revealed O-NEXOS as the most sensitive method, followed by E-NEXOS and SP-IRIS in third place (Figure 7). To the best of our knowledge, this study offers the first impartial comparison of the detection capabilities between a novel platform and established methodologies.

An unspoken advantage of NEXOS over the majority of sEV popular methods is its high-throughput format and minimal technical variability. All steps are conveniently performed in a 96-microtiter well plate and are compatible with automation. The exception is the step of detecting S-GNPs which occurs in E-NEXOS nanochips. The immunomagnetic capture of sEVs with MBs adds to its practicality and ensures an advantage over emerging technologies based on chip surface-based capture of sEVs.[28–30]

In liquid, effective mixing between the MBs and sEVs is facilitated, whereas surface-based techniques are constrained by the prolonged diffusion of target analytes onto a chip's surface.[31] As importantly, a strong limitation of assays requiring just one binding step to detect sEVs is the difficult distinction between sEVs and freely-circulating proteins and protein aggregates.

The E-NEXOS detection system surpasses the current state-of-the-art with its speed and simplicity.

It does not require any surface chemistry nor microfluidics which extends the nanochips shelf-life, scalability and user-friendliness. As the study shows, as long as a target sEV is bound to one S-GNP, the signal will be detected at the nanochip. This may result in its suitability for detecting sEV sub-types with scarce quantity of target surface markers.

Furthermore, the technology behind E-NEXOS has significant potential, as the number of nanogap-based sensors can be dramatically increased from 36 sensors up to 2 million sensors per nanochip, as demonstrated by various examples.[32–34]

E-NEXOS will eventually surpass the sensitivity of O-NEXOS significantly and achieve notable improvements in precision, dynamic range and throughput. The validation will be conducted using real clinical samples to evaluate the platform's potential in cancer diagnostics and explore its broader clinical use.

In conclusion, we envision the potential of NEXOS in both sEVs research and clinical applications. For example, the quantification of disease-specific epitopes (or proteins) per target sEV (TEPs/TEVs) may hold strong promise to drive precision medicine forward and advance the field of liquid biopsy diagnostics.[35–37]

Limitations of the study

We observed that at sEV concentrations lower than 7.5E6 particles/mL, the detected ratio of S-GNPs per sEV was underestimated. This is attributed to the limitations of the E-NEXOS nanochip, currently equipped with 36 sensors. This observation aligns with the findings that its linear range was between 7.5E6 particles/mL to 2.5E7 particles/mL. Nevertheless, E-NEXOS demonstrated the detection of sEVs down to 5E6 part/mL, despite not falling within its linear regime.

Validating the calculated epitope counts per target sEVs (TEPs/TEVs) posed a challenge and stands as one of the limitations of our study as currently, no technique can obtain such measurement. However, as our technologies share all pivotal steps from sEV capture to antibody binding, and with a maximum of two S-GNPs binding to one sEV in our assay, we hold confidence in this being one of the most promising strategies for advancing the field in this regard. Notably, with spiked plasma samples, both E-NEXOS and O-NEXOS signals exhibited similar reduction (2–2.5 times) compared to their performance with sEVs diluted in PBS (Figures 6B and 6C). Meanwhile, the calculated epitope count per sEVs remained constant regardless of PBS or plasma, further supporting our claims (Figure 6D). While our current study establishes a foundation for the NEXOS platform, we believe that further validation through comparative studies is crucial. In subsequent investigations, we plan to include detailed comparisons with parent cell epitope counts and alternative protein measurement methods to strengthen the reliability of our reported epitope counts. We also plan to investigate the intricacies of antibody interactions, considering factors such as steric hindrance and surface area constraints. This exploration will involve a comprehensive analysis of antibody binding kinetics and potential modifications to enhance the efficiency of epitope quantification into a reliable and universal approach.

STAR★METHODS

Detailed methods are provided in the online version of this paper and include the following:

- KEY RESOURCES TABLE
- RESOURCE AVAILABILITY
  - Lead contact
  - Materials availability
  - Data and code availability
- EXPERIMENTAL MODEL AND STUDY PARTICIPANT DETAILS
- METHODS DETAILS
  - Cell culture and sEVs preparation
  - Characterization of sEVs by nanoparticle tracking analysis
  - Western Blot analysis of sEV markers
  - Bead-based Flow Cytometry analysis of sEV markers
  - sEVs characterization by Transmission Electron Microscopy
  - E-NEXOS nanochip design and fabrication
  - Dielectrophoresis modeling in E-NEXOS
  - E-NEXOS nanochip interface and signal acquisition
  - Labeling of sEVs and mixing with MBs
  - Determination of $CD9^+$ sEVs capture rate and enrichment of $CD9^+CD81^+$ sEVs
  - E-NEXOS calibration, sEVs detection and determination of TEVs
  - O-NEXOS calibration and sEVs detection and determination of TEPs
  - Determination of LODs
  - Determination of TEVs and TEPs in BT-474 sEVs and plasma processing
- QUANTIFICATION AND STATISTICAL ANALYSIS

SUPPLEMENTAL INFORMATION

Supplemental information can be found online at https://doi.org/10.1016/j.isci.2024.109866.

ACKNOWLEDGMENTS

The authors would like to thank Prof. Crispin Barnes for welcoming selected team members from Mursla as visiting researchers in his research group at the Cavendish Laboratory of the University of Cambridge, to Prof. Andy Parker for supporting it and to Dr. Adrian Ionescu for his

technical guidance. The authors would further like to thank Prof. Yutaka Majima and Dr. Victor Serdio for the initial advancements in the nanochip developments, to Prof. Dr. Bernd Giebel and Amaury Genovese for revising the manuscript and Tobias Tertel for performing the IFC experiments, EverZom for performing the SP-IRIS experiments, Dr. Karin Müller from the Cambridge Advanced Imaging Center for her support and assistance in the imaging of sEVs by TEM, Thomas Mitchell and Jonathan Griffiths from Cavendish Laboratory for their support and services in EBL writing, Mr. Barry Shores from Cambridge University, Department of Physics for his support and services in electronics hardware design and interfacing, and finally to Prof. Andrea C. Ferrari of the Cambridge Graphene Center and Sue Murkett from The Nanoscience Center for allowing access to develop the nanochips. Figures 1, 4 and S1 were partially created with BioRender.com.

AUTHOR CONTRIBUTIONS

CASRAI CRediT Taxonomy: authors' contribution(s) to the submitted manuscript are attributed as follows: **T.D.:** Conceptualization-Lead, Data curation-Lead, Formal analysis-Lead, Investigation-Supporting, Methodology-Equal, Project administration-Lead, Resources-Equal, Software-Equal, Supervision-Lead, Validation-Equal, Visualization-Lead, Writing – original draft-Lead, Writing – review and editing-Lead; **R.F.**: Conceptualization-Supporting, Data curation-Supporting, Formal analysis-Supporting, Investigation-Equal, Methodology-Equal, Software-Supporting, Validation-Equal, Writing – original draft-Supporting, Writing – review and editing-Supporting; **S.V.**: Conceptualization-Supporting, Data curation-Supporting, Formal analysis-Supporting, Investigation-Equal, Methodology-Equal, Software-Supporting, Validation-Equal, Writing – original draft-Supporting, Writing – review and editing-Supporting; **R.D.**: Conceptualization-Supporting, Data curation-Supporting, Formal analysis-Supporting, Investigation-Equal, Methodology-Equal, Software-Supporting, Validation-Equal, Writing – original draft-Supporting, Writing – review and editing-Supporting; **Y.-H.H.**: Conceptualization-Supporting, Data curation-Supporting, Formal analysis-Supporting, Investigation-Supporting, Methodology-Supporting, Software-Supporting, Validation-Equal, Writing – original draft-Supporting, Writing – review and editing-Supporting; **J.S.**: Data curation-Supporting, Software-Supporting, Visualization-Supporting, Writing – review and editing-Equal; **E.P.:** Formal analysis-Supporting, Investigation-Supporting, Methodology-Supporting, Writing – original draft-Supporting; **P.A.:** Conceptualization-Supporting, Data curation-Supporting, Funding acquisition-Lead, Project administration-Equal, Resources-Lead, Writing – original draft-Supporting, Writing – review and editing-Supporting.

DECLARATION OF INTERESTS

All authors are or were employed by Mursla Bio and T.D., R.F., S.V., J.S., and E.P. hold share options at Mursla Bio. T.D., R.D., and P.A. are shareholders of Mursla Bio. P.A. is a founder of Mursla Bio and Chair of Exosla Ltd. T.D. is a member of the Scientific Advisory Board of EVCA. T.D. and P.A. have patents related to this work - GB2583550/Biosensor conditioning method and system; GB2595423/Biosensor conditioning method and system; US11738342B2/Biosensor activation and conditioning method and system; GB2601997B/Extracellular vesicle characterization systems.

DECLARATION OF GENERATIVE AI AND AI-ASSISTED TECHNOLOGIES IN THE WRITING PROCESS

During the preparation of this work, the authors used ChatGPT-4 in order to improve the readability and language of the manuscript. After using this tool or service, the authors reviewed and edited the content as needed and take full responsibility for the content of the publication.

Received: January 12, 2024
Revised: April 12, 2024
Accepted: April 29, 2024
Published: April 30, 2024

REFERENCES

1. Mathieu, M., Martin-Jaular, L., Lavieu, G., and Théry, C. (2019). Specificities of secretion and uptake of exosomes and other extracellular vesicles for cell-to-cell communication. Nat. Cell Biol. *21*, 9–17. https://doi.org/10.1038/s41556-018-0250-9.
2. Kalluri, R., and LeBleu, V.S. (2020). The biology, function, and biomedical applications of exosomes. Science *367*, eaau6977. https://doi.org/10.1126/science.aau6977.
3. Yates, A.G., Pink, R.C., Erdbrügger, U., Siljander, P.R.M., Dellar, E.R., Pantazi, P., Akbar, N., Cooke, W.R., Vatish, M., Dias-Neto, E., et al. (2022). In sickness and in health: The functional role of extracellular vesicles in physiology and pathology in vivo - PART I. J. Extracell. Vesicles *11*, e12151. https://doi.org/10.1002/jev2.12151.
4. Pink, R.C., Beaman, E.M., Samuel, P., Brooks, S.A., and Carter, D.R.F. (2022). Utilising extracellular vesicles for early cancer diagnostics: benefits, challenges and recommendations for the future. Br. J. Cancer *126*, 323–330. https://doi.org/10.1038/s41416-021-01668-4.
5. Herrmann, I.K., Wood, M.J.A., and Fuhrmann, G. (2021). Extracellular vesicles as a next-generation drug delivery platform. Nat. Nanotechnol. *16*, 748–759. https://doi.org/10.1038/s41565-021-00931-2.
6. Mørk, M., Handberg, A., Pedersen, S., Jørgensen, M.M., Bæk, R., Nielsen, M.K., and Kristensen, S.R. (2017). Prospects and limitations of antibody-mediated clearing of lipoproteins from blood plasma prior to nanoparticle tracking analysis of extracellular vesicles. J. Extracell. Vesicles *6*, 1308779. https://doi.org/10.1080/20013078.2017.1308779.
7. Ferguson, S., and Weissleder, R. (2020). Modeling EV Kinetics for Use in Early Cancer Detection. Adv. Biosyst. *4*, 1900305. https://doi.org/10.1002/adbi.201900305.
8. Arab, T., Mallick, E.R., Huang, Y., Dong, L., Liao, Z., Zhao, Z., Gololobova, O., Smith, B., Haughey, N.J., Pienta, K.J., et al. (2021). Characterization of extracellular vesicles and synthetic nanoparticles with four orthogonal single-particle analysis platforms. J. Extracell. Vesicles *10*, e12079. https://doi.org/10.1002/jev2.12079.

9. Imanbekova, M., Suarasan, S., Lu, Y., Jurchuk, S., and Wachsmann-Hogiu, S. (2022). Recent advances in optical label-free characterization of extracellular vesicles. Nanophotonics *11*, 2827–2863.
10. Nieuwland, R., and Siljander, P.R.M. (2024). A beginner's guide to study extracellular vesicles in human blood plasma and serum. J. Extracell. Vesicles *13*, e12400. https://doi.org/10.1002/jev2.12400.
11. Li, Y., He, X., Li, Q., Lai, H., Zhang, H., Hu, Z., Li, Y., and Huang, S. (2020). EV-origin: Enumerating the tissue-cellular origin of circulating extracellular vesicles using exLR profile. Comput. Struct. Biotechnol. J. *18*, 2851–2859. https://doi.org/10.1016/j.csbj.2020.10.002.
12. Hu, T., Wolfram, J., and Srivastava, S. (2021). Extracellular vesicles in cancer detection: hopes and hypes. Trends Cancer *7*, 122–133.
13. Kumar, S., Yoon, S.-H., and Kim, G.-H. (2009). Bridging the nanogap electrodes with gold nanoparticles using dielectrophoresis technique. Curr. Appl. Phys. *9*, 101–103. https://doi.org/10.1016/j.cap.2007.12.001.
14. Nasibeh Karimi, R.D., Dias, T., Lötvall, J., and Lässer, C. (2022). Tetraspanins distinguish separate extracellular vesicle subpopulations in human serum and plasma - Contributions of platelet extracellular vesicles in plasma samples. J. Extracellular vesicles *11*, e12213.
15. Welsh, J.A., Jones, J.C., and Tang, V.A. (2020). Fluorescence and light scatter calibration allow comparisons of small particle data in standard units across different flow cytometry platforms and detector settings. Cytometry A. *97*, 592–601.
16. Morales-Kastresana, A., and Jones, J.C. (2017). Flow cytometric analysis of extracellular vesicles. Methods Mol. Biol. *1545*, 215–225.
17. Mustapic, M., Eitan, E., Werner, J.K., Berkowitz, S.T., Lazaropoulos, M.P., Tran, J., Goetzl, E.J., and Kapogiannis, D. (2017). Plasma Extracellular Vesicles Enriched for Neuronal Origin: A Potential Window into Brain Pathologic Processes. Front. Neurosci. *11*, 278. https://doi.org/10.3389/fnins.2017.00278.
18. Popovic, M., Mazzega, E., Toffoletto, B., and de Marco, A. (2018). Isolation of anti-extracellular vesicle single-domain antibodies by direct panning on vesicle-enriched fractions. Microb. Cell Fact. *17*, 6. https://doi.org/10.1186/s12934-017-0856-9.
19. Shin, I. (2021). HER2 Signaling in Breast Cancer. In Translational Research in Breast Cancer, D.-Y. Noh, W. Han, and M. Toi, eds. (Springer Singapore), pp. 53–79. https://doi.org/10.1007/978-981-32-9620-6_3.
20. Ménard, S., Pupa, S.M., Campiglio, M., and Tagliabue, E. (2003). Biologic and therapeutic role of HER2 in cancer. Oncogene *22*, 6570–6578. https://doi.org/10.1038/sj.onc.1206779.
21. Théry, C., Witwer, K.W., Aikawa, E., Alcaraz, M.J., Anderson, J.D., Andriantsitohaina, R., Antoniou, A., Arab, T., Archer, F., Atkin-Smith, G.K., et al. (2018). Minimal information for studies of extracellular vesicles 2018 (MISEV2018): a position statement of the International Society for Extracellular Vesicles and update of the MISEV2014 guidelines. J. Extracell. Vesicles *7*, 1535750. https://doi.org/10.1080/20013078.2018.1535750.
22. Victor Serdio, T.D., and Arsène, P. (2020). GB2583550 - Biosensor Conditioning Method and System (UK).
23. Tomás Dias, P.A. (2021). GB2595423 - Biosensor Conditioning Method and System (UK).
24. Mugoni, V., Ciani, Y., Quaini, O., Tomasini, S., Notarangelo, M., Vannuccini, F., Marinelli, A., Leonardi, E., Pontalti, S., Martinelli, A., et al. (2023). Integrating extracellular vesicle and circulating cell-free DNA analysis using a single plasma aliquot improves the detection of HER2 positivity in breast cancer patients. J. Extracell. Biol. *2*, e108. https://doi.org/10.1002/jex2.108.
25. Hendrix, A., Lippens, L., Pinheiro, C., Théry, C., Martin-Jaular, L., Lötvall, J., Lässer, C., Hill, A.F., and Witwer, K.W. (2023). Extracellular vesicle analysis. Nat. Rev. Methods Primers *3*, 56. https://doi.org/10.1038/s43586-023-00240-z.
26. Welsh, J.A., Goberdhan, D.C.I., O'Driscoll, L., Buzas, E.I., Blenkiron, C., Bussolati, B., Cai, H., Di Vizio, D., Driedonks, T.A.P., Erdbrügger, U., et al. (2024). Minimal information for studies of extracellular vesicles (MISEV2023): From basic to advanced approaches. J. Extracell. Vesicles *13*, e12404. https://doi.org/10.1002/jev2.12404.
27. Kugeratski, F.G., Hodge, K., Lilla, S., McAndrews, K.M., Zhou, X., Hwang, R.F., Zanivan, S., and Kalluri, R. (2021). Quantitative proteomics identifies the core proteome of exosomes with syntenin-1 as the highest abundant protein and a putative universal biomarker. Nat. Cell Biol. *23*, 631–641. https://doi.org/10.1038/s41556-021-00693-y.
28. Kilic, T., Cho, Y.K., Jeong, N., Shin, I.-S., Carter, B.S., Balaj, L., Weissleder, R., and Lee, H. (2022). Multielectrode Spectroscopy Enables Rapid and Sensitive Molecular Profiling of Extracellular Vesicles. ACS Cent. Sci. *8*, 110–117. https://doi.org/10.1021/acscentsci.1c01193.
29. Hajian, R., DeCastro, J., Parkinson, J., Kane, A., Camelo, A.F.R., Chou, P.P., Yang, J., Wong, N., Hernandez, E.D.O., Goldsmith, B., et al. (2021). Rapid and Electronic Identification and Quantification of Age-Specific Circulating Exosomes via Biologically Activated Graphene Transistors. Adv. Biol. *5*, 2000594. https://doi.org/10.1002/adbi.202000594.
30. Qiu, G., Thakur, A., Xu, C., Ng, S.-P., Lee, Y., and Wu, C.-M.L. (2019). Detection of Glioma-Derived Exosomes with the Biotinylated Antibody-Functionalized Titanium Nitride Plasmonic Biosensor. Adv. Funct. Mater. *29*, 1806761. https://doi.org/10.1002/adfm.201806761.
31. Squires, T.M., Messinger, R.J., and Manalis, S.R. (2008). Making it stick: convection, reaction and diffusion in surface-based biosensors. Nat. Biotechnol. *26*, 417–426. https://doi.org/10.1038/nbt1388.
32. Fuller, C.W., Padayatti, P.S., Abderrahim, H., Adamiak, L., Alagar, N., Ananthapadmanabhan, N., Baek, J., Chinni, S., Choi, C., Delaney, K.J., et al. (2022). Molecular electronics sensors on a scalable semiconductor chip: A platform for single-molecule measurement of binding kinetics and enzyme activity. Proc. Natl. Acad. Sci. USA *119*, e2112812119. https://doi.org/10.1073/pnas.2112812119.
33. Hall, D.A., Daniels, J.S., Geuskens, B., Tayebi, N., Credo, G.M., Liu, D.J., Li, H., Wu, K., Su, X., Varma, M., and Elibol, O.H. (2016). 16.1 A Nanogap Transducer Array on 32nm CMOS for Electrochemical DNA Sequencing (IEEE), pp. 288–289.
34. Huang, M., Chang, T., Yanik, A.A., Tsai, H., Shi, P., Aksu, S., Yanik, M.F., and Altug, H. (2012). Large-scale Plasmonic Microarray: A New Approach for Label-free High-Throughput Biosensing and Screening (IEEE), pp. 1–2.
35. Hoshino, A., Kim, H.S., Bojmar, L., Gyan, K.E., Cioffi, M., Hernandez, J., Zambirinis, C.P., Rodrigues, G., Molina, H., Heissel, S., et al. (2020). Extracellular Vesicle and Particle Biomarkers Define Multiple Human Cancers. Cell *182*, 1044–1061.e18. https://doi.org/10.1016/j.cell.2020.07.009.
36. Rontogianni, S., Synadaki, E., Li, B., Liefaard, M.C., Lips, E.H., Wesseling, J., Wu, W., and Altelaar, M. (2019). Proteomic profiling of extracellular vesicles allows for human breast cancer subtyping. Commun. Biol. *2*, 325. https://doi.org/10.1038/s42003-019-0570-8.
37. Trino, S., Lamorte, D., Caivano, A., De Luca, L., Sgambato, A., and Laurenzana, I. (2021). Clinical relevance of extracellular vesicles in hematological neoplasms: from liquid biopsy to cell biopsy. Leukemia *35*, 661–678. https://doi.org/10.1038/s41375-020-01104-1.

STAR★METHODS

KEY RESOURCES TABLE

REAGENT or RESOURCE	SOURCE	IDENTIFIER
Antibodies		
Anti-ErbB2/HER2 antibody [3B5]	Abcam	ab16901; RRID: AB_443537
Anti-TSG101 antibody [4A10]	Abcam	ab83; RRID: AB_306450
Anti-CD63 antibody [TS63]	Abcam	ab59479; RRID: AB_940915
anti-CD81 antibody	Biorbyt	Cat# orb506485
Mouse IgG1 Kappa Isotype control Antibody	Biorbyt	Cat# orb343761
Anti-CD9 antibody [TS9]	Abcam	ab58989; RRID: AB_940926
Mouse IgG Horseradish Peroxidase-conjugated Antibody	R&D systems	HAF007; RRID: AB_357234
Anti-CD81 antibody [TS81]	Abcam	ab59477; RRID: AB_943630
Biotin Anti-CD81 antibody [M38]	Abcam	ab239238
Mouse IgG1, kappa monoclonal [15-6E10A7] - Isotype Control	Abcam	ab170190; RRID: AB_2736870
Streptavidin-Phycoerythrin (R-PE)	Abcam	ab239759
Human IgG Isotype Control [Biotin]	Novus Biological	NBP1-96855
Goat Anti-Mouse IgG H&L (Alexa Fluor® 488)	Abcam	ab150113; RRID: AB_2576208
ErbB2/Her2 Biotinylated Antibody	R&D systems	Cat# FAB9589B; RRID: AB_2934015
Biological samples		
Healthy human plasma (in K2EDTA)	Cambridge bioscience	Cat# PLS1DF2EDT12-XS
Chemicals, peptides, and recombinant proteins		
10X RIPA lysis buffer	Abcam	ab156034
Halt™ Protease Inhibitor Cocktail	Thermofisher Scientific	Cat# 78429
NuPAGE™ LDS Sample Buffer (4X)	Invitrogen (Thermofisher Scientific)	Cat# NP0008
NuPAGE™ Sample Reducing Agent (10X)	Invitrogen (Thermofisher Scientific)	Cat# NP0004
SuperSignal™ West Pico PLUS Chemiluminescent Substrate	Thermofisher Scientific	Cat# 34580
Dynabeads™ M-270 Epoxy	Invitrogen (Thermofisher Scientific)	Cat# 14301
Streptavidin - 200nm Gold Conjugate	Cytodiagnostics	N/A
Pierce™ Streptavidin Poly-HRP	Thermofisher Scientific	Cat# 21140
QuantaBlu™ Fluorogenic Peroxidase Substrate Kit	Thermofisher Scientific	Cat#15169
Critical commercial assays		
ExoELISA Complete Kit (CD81 Detection)	Systems Biosciences	N/A
Experimental models: Cell lines		
Human: MCF-7	ATCC	HTB-22
Human: BT-474	ATCC	HTB-20
Deposited data		
Original Western Blots	This paper	https://doi.org/10.17632/69fkfdxx5j.1
Immunomagnetic assay characterization	This paper	https://doi.org/10.17632/drvyxcpwrj.1
Original O-NEXOS data - BT-474 sEVs detection	This paper	https://doi.org/10.17632/nhm7syydc6.1
Original sEVs detection data - comparative analysis	This paper	https://doi.org/10.17632/pyd3pckg5n.1
Software and algorithms		
ImageJ	National Institutes of Health	https://imagej.nih.gov/ij/
COMSOL Multiphysics	COMSOL	https://www.comsol.com/comsol-multiphysics

(*Continued on next page*)

Continued

REAGENT or RESOURCE	SOURCE	IDENTIFIER
OriginLab	OriginLab	https://www.originlab.com/
BioRender	Biorender	https://www.biorender.com/
Microsoft Excel	Microsoft	https://www.microsoft.com/en-gb/microsoft-365/excel
FlowJo Software v10.6.1	FLOWJO	https://www.flowjo.com/solutions/flowjo/downloads
Other		
Izon qEV original/70 nm columns	IZON	Product code: IC1-70
Readout system (E-NEXOS)	TronicsZone	N/A

RESOURCE AVAILABILITY

Lead contact

Further information and requests for resources should be directed to the Lead Contact, Tomás Dias (tomas.dias@mursla.com)

Materials availability

This study did not generate new unique reagents.

Data and code availability

- This paper does not report original code except for the firmware, software and interface of E-NEXOS.
- The original western blot images, BCA data, NTA data, O-NEXOS data, TEPs per TEV, ELISA data, IFC data, and SP-IRIS data have been deposited at Mendeley and are publicly available as of the date of publication. The DOI is listed in the key resources table. Electrical data reported in this paper can be shared by the lead contact upon request.
- Any additional information required to reanalyse the data reported in this paper is available from the lead contact upon request.

EXPERIMENTAL MODEL AND STUDY PARTICIPANT DETAILS

Breast cancer cell lines MCF-7 (ATCC, catalog nr HTB-22) and BT-474 (ATCC, catalog nr HTB-20) were grown in growth medium Advanced-DMEM (Gibco), supplemented with 5% (v/v) FBS (Gibco) and 4 mM glutaMAX (Gibco), in a humidifying atmosphere with 5% CO_2 and 37°C. These cells were acquired from ATCC and freshly preparing according to the instructions provided.

The study involved plasma from human participants. 4 mL fresh human plasma derived from whole blood in K2EDTA Vacutainers was acquired (Cambridge bioscience). The human plasma was ethically consented and originated from a pool of healthy, paid volunteers (Research Donors).

METHODS DETAILS

Cell culture and sEVs preparation

Breast cancer cell lines MCF-7 (ATCC, catalog nr HTB-22) and BT-474 (ATCC, catalog nr HTB-20) were grown in growth medium Advanced-DMEM (Gibco), supplemented with 5% (v/v) FBS (Gibco) and 4 mM glutaMAX (Gibco), in a humidifying atmosphere with 5% CO_2 and 37°C.

After reaching 70% confluency in T175 flaks (ThermoFisher), the cells were gently washed three times with PBS and were cultured in Advanced-DMEM FBS-free medium.

After 48h, the conditioned medium (CM) was collected and centrifuged for 5 min at 300 *g*, followed by another centrifugation of 10 min at 3000 *g* and 4°C to remove cellular debris and other large contaminants.

The CM was then filtered using 0.22 μm PES filters (FisherBrand) and concentrated 220 x down to 500 μL with Amicon Ultra-15 100K MWCO Centrifugal filters (Merck Millipore).

By size exclusion chromatography (SEC), the sEVs were finally isolated using Izon qEV original/70 nm columns (IZON), on an Automatic Fraction Collector (AFC), according to the supplier's instructions.

The first eluted three fractions, corresponding to a total of 1.5 mL of elution volume, were collected, pooled together, aliquoted in volumes of 50 μL and stored at −80°C until further use.

Characterization of sEVs by nanoparticle tracking analysis

Particle number and size distribution of MCF-7 and BT-474 and sEV preparations was determined by Nanoparticle Tracking Analysis (NTA) using a NanoSight NS300 system (Malvern) configured with a 488 nm laser and a high sensitivity scientific CMOS camera.

Samples were diluted in particle-free PBS (Gibco), to an acceptable concentration, according to the manufacturer's recommendations, to an average of 50 particles/frame for the measurements. The samples were analyzed under constant flow rate and 3 × 60 s videos were captured with a camera level of 12. Data was analyzed using NTA 3.4 software with a detection threshold of 7.

Western Blot analysis of sEV markers

MCF-7 and BT-474 sEV preparations were normalized to a concentration of 1E10 part/mL by dilution in particle-free PBS (ThermoFisher). Then, 100 μL of each sample was lysed in 1 x RIPA lysis buffer (ab156034, Abcam) supplemented with 1 x Halt Protease Inhibitor Cocktail (Thermo Fisher) and incubated for 1 h on ice followed by 2 × 30 s sonication in ice-cold water.

After, the samples were mixed with NuPAGE LDS Sample Buffer (4X) (Invitrogen) and NuPAGE Sample Reducing Agent (10X) (Invitrogen).

After boiling for 10 min at 70°C, 37 μL per sample was loaded on a NuPAGE 4 to 12%, Bis-Tris, 1.0–1.5 mm, Mini Protein Gels (Invitrogen). Electrophoresis occurred at 150 V, using MES as the running buffer. Protein ladders (26634, Thermo Scientific orLC5925, Invitrogen) were run along with the sEV samples.

Transfer was performed on PVDF membranes (IB24002, Invitrogen) using an iBlot 2 Dry Blotting System (Invitrogen).

Using an iBind Western Device (Thermo Fisher) and following the supplier instructions, the membranes were incubated sequentially with iBind solution for blocking, primary antibodies and secondary antibody. The primary antibodies used were anti-HER2 (ab16901, Abcam) at 1:400, anti-TSG101 (ab83, Abcam) at 1:700, anti-CD63 (ab59479, Abcam) at 1:1000, anti-CD81 (orb506485, Biorbyt) at 1:1000 or anti-CD9 (ab58989, Abcam) at 1:1000. The secondary antibody used was a secondary antibody anti-mouse (HAF007, R&D Systems) at 1:250 dilution.

Finally, membranes were subsequently incubated with SuperSignal West Pico PLUS. Chemiluminescent Substrate (Thermo Scientific) and the bands were visualized and acquired on a GBOX Chemi XRQ (Syngene).

Bead-based Flow Cytometry analysis of sEV markers

MCF-7 and BT-474 sEVs were characterized by bead-based Flow Cytometry (FCM) to further validate the presence of CD63, CD81, CD9, and HER2 in the sEVs preparations. The sEVs were attached to 4 μm aldehyde/sulfate latex beads (Invitrogen) by the mixing of 8E8 sEVs with 4E6 beads in 200 μL of PBS for 20 min with continuous rotation.

The suspensions were diluted to 300 μL with PBS and left incubating overnight under agitation. The reactions were stopped with 100 mM glycine in PBS, during 1 h and under continuous agitation. Bead-bound sEVs were centrifuged for 5 min at 12000 *g* and the PBS was replaced once. The bead-bound sEVs were centrifuged again for 5 min at 12000 *g*, supernatant was discarded and bead-bound sEVs were blocked by resuspension of the beads in 300 μL of PBS with 5% BSA. After 45 min of agitation, the beads were washed a second time in 2% BSA and centrifuged once more for 5 min at 12000 *g*, and resuspended with primary antibodies either targeting CD63, CD81, CD9 or HER2, in 2% BSA for 1 h with rotation. Samples were washed three times in 200 μL of 2% BSA and incubation with secondary antibody was done in the dark for 30 min, washed as previously described and resuspended in 600 μL 2% BSA.

For tetraspanins detection, the mouse antibodies anti-CD63 (ab59479, Abcam), anti-CD81 (ab59477, Abcam) or anti-CD9 (ab58989, Abcam) were used. HER2 was detected with a recombinant human biotinylated antibody (FAB9589B, RnDSystems). Mouse isotype antibody (ab170190, Abcam) or human isotype biotinylated (NBP1-96855, Novus Biological) were used as controls. Secondary antibody anti-mouse AF488 (ab150113, Abcam) or PE-streptavidin (ab239759, Abcam) were used as reporters.

Analysis was performed by FCM using an Invitrogen Attune NxT. The channel YL1 (excitation 561 nm and emission 585/16 nm) or BL1 (excitation 488 nm and emission 530/30nm) were selected for detection of the PE or AF488 fluorophores, respectively. Results were visualized using Invitrogen Attune NxT Software. Single sEVs-beads complexes were gated using forward-scattered light (FSC) Area (A) (x axis) and side-scattered light (SSC) Area (A) (y axis). Data analysis was performed with FlowJo Software v10.6.1. The percentage of positive beads was calculated relative to the total number of beads analyzed per sample (10,000 events). This percentage was therein referred to as the percentage of beads with sEV markers.

sEVs characterization by Transmission Electron Microscopy

10 μL of freshly prepared sEVs at a concentration of 1E9 part/mL were spotted on a glow-discharged carbon-coated 400 mesh copper TEM grid and incubated for 2 min. To remove excess PBS, the TEM grid was washed in 2 consecutive 10 μL drops of deionized water for 30s each.

Then, the grid was stained with 10 μL of uranyl acetate for 60 s. The grid was dried by tapping it on dust-free clean room paper. Finally, the grid was transferred to a FEI Tecnai G2 TEM and imaged at room temperature and 200 kV. Images were acquired with a bottom-mounted AMT CCD camera, using a bright field imaging mode.

E-NEXOS nanochip design and fabrication

The nanochips were designed on AutoCAD and fabricated on n-doped silicon 4″ wafers of 525 μm thickness, coated with 100 nm WET thermal oxide. The design included 37 dyes, each one corresponding to one E-NEXOS nanochip, with a separation of 360 μm between each dye.

The fabrication was divided into two layers, each with a lithography and metal deposition steps.

The nanogaps were fabricated in the first layer. First, 100 nm thick PMMA 950K A4 positive resist was spin-coated on the substrate. Then, the resist was exposed by electron beam lithography at a dose of 590 $\mu C/cm^2$ (Vistec VB6) and developed in a solution made of IPA:MIBK:MEK

15:5:1. After development, Ti 5/Au 30 (thicknesses in nm) were deposited by electron-beam evaporation (Lesker e-beam evaporator PVD 200 Pro) and the gold-patterned nanogaps were revealed by lift-off in acetone.

The contact lines and pads were fabricated in the second layer. AZ5214-E 1000 nm thick image reversal photoresist was spin-coated on the substrate. The pattern was exposed and defined by photolithography (SUSS Microtech MA/BA6 mask aligner) with critical dimension <2 μm. The photoresist layer was developed in an aqueous solution of H_20:AZ351B 4:1. After development, Ti 5/Au 30 (in nm) layers were deposited, again, by evaporation using the Lesker PVD 200 Pro, followed by lift-off using AZ100.

Finally, the wafers were diced into 37 nanochips using a mechanical dicer (DISCO DAD341) and the nanogaps were quality-checked by room temperature SEM (FEI Magellan 400L) ETD detector at 5 kV, with secondary electrons imaging, to confirm the physical separation and dimensions of the structures. Additionally, after using E-NEXOS, the presence of S-GNPs on selected sensors was also visualized by SEM.

Dielectrophoresis modeling in E-NEXOS

We designed a 3D finite element model using COMSOL Multiphysics to determine the electric field characteristics around the nanogap and the dieletrophoresis (DEP) force exerted on a double-shell gold nanoparticle simulating the S-GNPs used in our experiments.

The model comprised a 12 μm × 12 μm x 8 μm simulation block with 2 gold electrodes of 300 nm width and 35 nm thickness separated by 50 nm and sitting on top of a SiO_2 substrate. The model considered the effective complex Clausius-Mossoti factor of an S-GNP with a gold core (200 nm) and 2 shell layers (thiol and streptavidin), suspended in deionized water.

The cross-sectional gradient of the electric field intensity was simulated over the 3 orthogonal planes across the nanogap using COMSOL's Electrostatics module. We fixed 0 V in one of the electrodes, and the quadratic mean of 2 V in the other electrode (as we used experimentally).

E-NEXOS nanochip interface and signal acquisition

The nanochips were interfaced with a dedicated readout system designed and developed by TronicsZone. The interface occurred via a plug-in printed circuit board (PCB) developed by Newbury Electronics Ltd, which connects the E-NEXOS nanochip and the readout system via spring-loaded pins. The readout was used for sourcing DC/AC to the nanochips and for measuring DC currents after the trapping of S-GNPs on the nanogaps.

The sensing area of the nanochips was protected from exterior wiring or contact with the PCB with barriers made of elastosil E−41 (Wacker).

For signal acquisition, several steps were performed. First, sequential IV curves on every sensor (0-5V), defined the sensors baseline. Sensors with current leakages above 50 nA were excluded. Then, 45 μL of S-GNPs suspensions, prepared as explained before, were pipetted over the sensing area and DEP was performed at 2 V AC and 100 kHz for 60s in every sensor.

After DEP, the solution was blown-dried with pressurized filtered air. Subsequently, we applied an activation step of 5 V for 20s, followed by an IV curve (0-5V), sequentially in every sensor. The sensors with current readings under 1 μA were counted as disconnected. Data analysis was automated with a script developed in Python.

Labeling of sEVs and mixing with MBs

sEVs were thawed on ice and diluted to target sEV concentrations, ranging from 1E8 down to 5E5 part/mL in a final buffer composition of 1 x PBS, 0.1% BSA, 0.02% Tween20. 100 ng of detection antibodies anti-CD81 (ab239238, Abcam) or anti-HER2 (FAB9589B-100, R&D Systems) were added to each sEV sample totalling a final total volume of 200 μL per well in a U-shaped 96-well plate and incubated for 45 min at RT and 200 RPM. Magnetic beads (MBs) (Dynabeads M-270 Epoxy beads), were coupled to sEVs capture antibodies anti-CD9 (ab58989, Abcam), anti-CD81 (orb506485, Biorbyt) or isotype IgG (orb343761, Biorbyt), by using the Dynabeads Antibody Coupling Kit whilst following the supplier's instructions. Briefly, the MBs were washed as per the kit instructions and incubated ON at 37°C, under constant rotation in LoBind microcentrifuge tubes (Eppendorf). The amount of capture antibody used in the reactions was 10 μg per mg of MBs. Tween20 (0.05%) was added in HB and LB wash buffers for improved stringency as recommended by the supplier. Washings of the MBs was performed with a DynaMag – Spin Magnet (Invitrogen).

7.5 μL or 15 μL of MBs, were added to the sEVs diluted in PBS or sEVs spiked in processed plasma, respectively. The capture of sEVs by the MBs occurred for 3 h with a step of up-and-down pipetting every 30 min to guarantee the homogeneous mixing of the MBs and the sEVs with the aid of an automatic pipetting robotic (Opentrons). After, the MBs were washed three times in PBS with 0.05% Tween20 and 0.1% BSA before proceeding for detection in E-NEXOS or O-NEXOS.

Determination of $CD9^+$ sEVs capture rate and enrichment of $CD9^+CD81^+$ sEVs

To determine the capture rate of sEVs by the MBs, MCF-7 sEVs were captured with MBs pre-coated with antibody anti-CD9 as explained before. As opposed to the prior methods, a detection antibody was not used to pre-label the sEVs. After an incubation period of 3 h, the MBs-bound sEVs were washed in a magnetic field, buffer was removed and the sEVs were eluted from the MBs in 0.2 M Glycine, pH 2.6 0.05% Tween20 (equal v/v Glycine solution to MBs). The pH was restored to pH 7.2 with 1 M Tris-HCL, pH 9.0 (1 μL of TRIS per 10 μL of Glycine). Then, the concentration of sEVs was determined by NTA. Enriched $CD9^+$ sEVs, at a concentration of 7.29E9 part/mL, were captured again with MBs anti-CD9. The concentration of sEVs remaining in the supernatant was determined by NTA.

To specifically enrich for $CD9^+CD81^+$ sEVs, MCF-7 sEVs, were first captured with MBs anti-CD9 and eluted in glycine solution as previously, and captured again with MBs anti-CD81 and eluted once again in glycine solution. Then, we serially diluted the enriched $CD9^+CD81^+$ sEVs to samples starting at a concentration of 1E8 part/mL down to 1E6 part/mL.

E-NEXOS calibration, sEVs detection and determination of TEVs

The concentration of S-GNPs was determined by NTA. Then, a suspension with S-GNPs at a concentration of 2E9 part/mL was serially washed thrice by centrifugation for 15 min at 400 *g* and resuspended in either 1% PBS (high range mode) or ultra-pure water (low range mode). The S-GNPs where the buffer was exchanged to 1% PBS, were serially diluted to concentrations ranging from 1E8 part/mL down to 1E6 part/mL by the addition of 1% PBS in a volume of 200 μL per sample. Otherwise, the S-GNPs where the buffer was exchanged to ultra-pure water, were serially diluted to concentrations ranging from 2.5E6 part/mL down to 7E4 part/mL by addition of ultra-pure water, again, in a volume of 200 μL per sample. After, 45 μL of each sample were pipetted onto the E-NEXOS nanochips and corresponding signal was acquired. A calibration curve was derived, allowing to correlate the number of hits with the concentration of S-GNPs in solution. Samples with serially diluted sEV concentrations were labeled with detection antibodies (i.e., anti-CD81 or anti-HER2) and captured with MBs anti-CD9, as previously explained. After incubation, the MBs were washed in 1 x PBS, 0.1% BSA, 0.02% Tween20 under a magnetic field. The buffer was removed and 200 μL of 2E9 part/mL S-GNPs were added to the samples and incubated for 30 min under constant agitation. Unbound S-GNPs were washed away and sEV-bound S-GNPs were finally eluted in Glycine, pH 2.6 0.05% Tween20 (equal v/v Glycine solution to MBs). The pH was restored to pH 7.2 and then exchanged to either 1% PBS or ultra-pure water. A volume of 45 μL per sample was pipetted onto the E-NEXOS nanochips for signal acquisition.

For the determination of TEVs, we serially diluted samples enriched in $CD9^+CD81^+$ MCF-7 sEVs, prepared as previously explained. The percentage of E-NEXOS hits was determined for each concentration and a calibration curve was derived, enabling to correlate the concentration of S-GNPs with the concentration of TEVs.

O-NEXOS calibration and sEVs detection and determination of TEPs

To calibrate O-NEXOS, Pierce Streptavidin poly-HRP (S-polyHRP) (Thermo Scientific) was diluted 1:6000 in 1 x PBS, 0.1% BSA, 0.02% Tween20, corresponding to 9.12E11 streptavidin molecules/mL. Then, S-polyHRP was serially diluted into several lower concentrations. 10 μL of each concentration was transferred into a U-shaped 96-well plate and incubated with 100 μL QuantaBlu Fluorogenic Peroxidase Substrate Kit (Thermo Scientific) for 40 min along with the sEV samples to be detected in O-NEXOS. The reactions were stopped by adding 100 μL of stop solution and 190 μL of each sample was transferred to an F-shaped 96-well plate. Fluorescence signals were obtained at Ex/Em = 320/405 nm with a Fluoroskan Ascent FL Microplate Fluorometer (Thermo Scientific).

Samples of serially diluted concentrations of sEVs were labeled with detection antibodies and captured with MBs anti-CD9.

Final buffer was removed and 200 μL of S-polyHRP (1:6000 dilution) was added and incubated for 30 min. After washing, and as for the calibration of O-NEXOS, 100 μL QuantaBlu was added and the reaction was stopped after 40 min.

A volume of190 μL of each sample was transferred to an F-shaped 96-well plate for signal measurement at Ex/Em = 320/405 nm.

The calibration curve enabled correlating the fluorescence signal with the concentration of S-polyHRP molecules in a solution but these could not be directly converted to TEPs in sEV samples. For that conversion, we inputted the stoichiometric linking between different molecules in the assay.

IgG antibodies (used in the study) have two identical antigen-binding sites which, at any instance, can be either attached to one or two target epitopes on sEV surface proteins. Additionally, S-polyHRP (with a 6:1 ratio of HRPs to Streptavidin, as provided by the supplier) has up to four biotin-binding sites and can link with up to four biotinylated antibodies. This results in different binding scenarios where each S-polyHRP could be bound to 1, 8, or any number of TEPs in between.

Therefore, we determined the mean of the eight different possible events and their standard deviation which resulted in a Gaussian distribution centered around 4.5 TEPs per S-polyHRP with a standard deviation of 2.3 (Equation 2).

Determination of LODs

To compare the sensitivity of O-NEXOS and E-NEXOS with some of the popular technologies, BT-474-derived sEVs were serially diluted in PBS to concentrations in the range of 5E8 and 7.5E5 part/mL, and several aliquots with 200 μL were stored in protein LoBind tubes (Eppendorf) at −80°C. Aliquots were shipped in dry ice to EVerZom and the Giebel Lab, for sEV measurements via SP-IRIS ($CD9^+CD81^+$ and CD9+HER2+ sEVs) or IFC ($CD81^+$ and HER2+ sEVs), respectively. The LOD of the techniques was determined for the aforementioned sEV sub-populations. Remaining aliquots were used for the measurement and LOD determination of E-NEXOS, O-NEXOS and ELISA. The colorimetric ExoELISA-ULTRA Complete ELISA Kit (Systems Biosciences) was used for CD81 detection according to the supplier's instructions.

Determination of TEVs and TEPs in BT-474 sEVs and plasma processing

TEVs and TEPs were calculated via the procedure explained in previous sections.

Additionally, 4 mL fresh human plasma derived from whole blood in K2EDTA Vacutainers was acquired (Cambridge bioscience). The human plasma was ethically consented and originated from a pool of healthy, paid volunteers (Research Donors).

The human plasma was slowly thawed on ice and divided into two portions of 2 mL each. One of the portions was spiked with BT-474 sEVs, to a final concentration of 1.67E9 part/mL. Then, both the spiked and non-spiked samples were treated in an equal manner with a centrifugation step at 3000 *g*, at 4°C for 15 min, followed by another centrifugation of 20 min at 10000 *g* and 4°C to remove any cell debris, large particles or aggregates.

Finally, we serially diluted the processed spiked plasma to BT-474 sEV concentrations of 1E8, 5E7, 2.5E7, 1E7, 5E6 and 2.5E6 by the addition of non-spiked processed plasma.

QUANTIFICATION AND STATISTICAL ANALYSIS

All of statistical details of experiments can be found in the figure legends, including the exact value of n (conditions). These represent the number of technical replicates used in each experiment.